

Title	Spectral, tensor, and ab initio theoretical analysis of optical second harmonic generation from the rutile TiO ₂ (110) and (001) faces
Author(s)	Omote, M.; Kitaoka, H.; Kobayashi, E.; Suzuki, O.; Aratake, K.; Sano, H.; Mizutani, G.; Wolf, W.; Podloucky, R.
Citation	Journal of Physics: Condensed Matter, 17(8): S175-S200
Issue Date	2005-03-02
Type	Journal Article
Text version	author
URL	http://hdl.handle.net/10119/4465
Rights	Copyright (c) Institute of Physics and IOP Publishing Limited 2005. This is the author-created version of Institute of Physics and IOP Publishing Limited, M. Omote, H. Kitaoka, E. Kobayashi, O. Suzuki, K. Aratake, H. Sano, G. Mizutani, W. Wolf, and R. Podloucky, Journal of Physics: Condensed Matter, 17(8), 2005, S175-S200.
Description	

Spectral, tensor, and *ab initio* theoretical analysis of optical second harmonic generation from the rutile TiO₂(110) and (001) faces

M. Omote, H. Kitaoka, E. Kobayashi^{*}, O. Suzuki, K. Aratake, H. Sano, G. Mizutani^{**}

Japan Advanced Institute of Science and Technology, Tatsunokuchi, Ishikawa 923-1292, Japan

W. Wolf

Materials Design s.a.r.l., 44, av. F.-A. Bartholdi, 72000 Le Mans, France

R. Podloucky

Institute of Physical chemistry, University of Vienna, Liechtensteinstrasse 22A, A 1090 Vienna, Austria

We overview our recent experimental study on the optical second harmonic (SH) response of the rutile TiO₂(110) and (001) faces, and the analysis of these results by phenomenological electromagnetic theory using nonlinear susceptibility tensors and by *ab initio* theory using the self-consistent full potential linearized augmented plane-wave (FLAPW) method within the local-density approximation. Since bulk rutile TiO₂ has a uniaxial crystal structure of symmetry D_{4h}^{14} , nonlinear optical response of its surface and bulk showed remarkable anisotropy. The TiO₂(110) face exhibited stronger reflected SH response when the incident electric field was directed parallel than perpendicular to the [001] axis, while the TiO₂(001) face exhibited relatively isotropic SH response. The anisotropy of the SH intensity patterns depended remarkably on the incident photon energy and the polarization combination. By using a phenomenological electromagnetic theory, we performed a simultaneous analysis of the SH intensity patterns from the (110) and (001) faces as a function of the sample rotation angle around its surface normal. As a

result we could separate the contributions from the surface second-order and bulk higher order nonlinear susceptibilities. We also found that the SH intensity spectra as a function of the SH photon energy depended strongly on the sample rotation angle and the polarization combination of the fundamental and SH light. The onset of the SH resonance of the $\text{TiO}_2(110)$ face was located at $2\eta\omega \sim 3.4$ eV when the induced nonlinear polarization was perpendicular to the surface. It was located at $2\eta\omega \sim 3.2$ eV when the induced nonlinear polarization is parallel to the $[001]$ direction in the surface plane. These onset energies were higher than the onset energy of the bulk linear absorption at 3.0eV. On the other hand, the onset energy of the SH resonance of the (001) face was found at $2\eta\omega \sim 3.0$ eV. Discussion was given on the physical meaning of the observed SH intensity spectra. Furthermore, *ab initio* calculation of the nonlinear optical response from the $\text{TiO}_2(110)$ surface using the FLAPW method was performed. The calculated results agreed very well with the experimental SH intensity patterns and spectra. We found both from the phenomenological and *ab initio* calculation that the main SH response from the $\text{TiO}_2(110)$ surface originated from the Ti-O-Ti-O- zigzag chains on the $\text{TiO}_2(110)$ surface.

Keywords : surface optical second harmonic generation, rutile $\text{TiO}_2(110)$, (001), photocatalyst, *ab initio* calculation

****Corresponding author** : G. Mizutani,

Japan Advanced Institute of Science and Technology, Tatsunokuchi, Ishikawa 923-1292, Japan

Fax : +81-761-51-1149, E-mail : mizutani@jaist.ac.jp

***Present address:** Institute of Materials Structure Science, 1-1 Oho, Tsukuba, Ibaraki 305-0801,
Japan

1. Introduction

Optical second harmonic (SH) spectroscopy has emerged as a new tool for the analyses of surfaces and interfaces of solid state materials [1][2][3][4]. By using the surface and interface specificity and resonance profile of second harmonic generation (SHG), we can find distribution of surface and interface electronic levels on the energy scale in the band structure. By using the strong anisotropy of the SH response from asymmetric atomic bonds, we can find information on the surface and interface structures including those with adsorbates. This nonlinear optical technique offers us several significant advantages over the conventional surface spectroscopies as in the followings: Unlike the method using electron or ion beams, it is free of material damage and contamination associated with charged particles. Sample surfaces in reaction in gaseous environment are accessible and so are the buried interfaces under optically transparent materials. Insulators can be studied without a problem of charging effects. For example, stoichiometric TiO_2 investigated in this study is an insulator and its surface electronic states cannot be studied in principle by ion or electron probes due to the charge up effect, while it can be studied with no problem by second harmonic spectroscopy. Also in SH spectroscopy one can take advantage of the excellent spectral and temporal resolution given by the well-developed pulsed lasers or coherent light sources.

In spite of these advantages, the analysis of the anisotropy and the spectra of SH intensity of solid state material surfaces is not easy and have not been performed prevalently. Only a

limited number of attempts of systematic analyses have been made so far [5][6][7][8]. The separation of the contribution from the surface and bulk nonlinear susceptibility elements $\chi_{Sijk}^{(2)}$ and Γ_{ijkl} is difficult, because the number of these susceptibility elements are generally large. For media without bulk inversion symmetry, strong bulk dipolar SH response overwhelms the surface response, so we have to choose special configurations to suppress the bulk [9]. For centrosymmetric media like TiO_2 studied in this work, the strong bulk dipolar SH response is absent but higher-order electromagnetic multipoles cause a weak bulk SH radiation [10][11].

The basic formulation of the analysis of SH intensity is straightforward, according to the framework developed in the textbook by Bloembergen [12]. However, for anisotropic materials like TiO_2 the analysis of the second harmonic intensity is complicated. In an anisotropic medium, the incident electric field is split into two electromagnetic fields known as ordinary and extraordinary waves due to the birefringence effect. When we calculate its nonlinear optical response we must consider the birefringence effect both for incident and second harmonic waves. Some of the works have gone into details of this treatment for anisotropic media [13][14][15][16]. However, there has been no example of a systematic and simultaneous analysis of SH intensity patterns and spectra for an anisotropic nonlinear surface. In this study we are giving such a demonstration for titanium dioxide TiO_2 , a material also well-known as a photo-catalyst working under UV light illumination.

The surface or interface electronic states of a photo-catalytic material is very important to

investigate. For this purpose SH spectroscopy is a good candidate tool because photo-catalyst usually works in a gaseous environment. In fact we have pointed out in our previous study that the SH intensity changes as the TiO_2 interface is illuminated with UV light [17][18]. In order to analyze such a phenomenon and get information on the working electronic states, a thorough scrutiny and basic understanding of the nonlinear optical phenomena in this material not only with but also without UV light illumination is important. This study is focused on the latter case as a first step of such a study.

In our previous papers we performed a tentative analysis of the SH intensity patterns from rutile $\text{TiO}_2(110)$ as a function of the azimuthal angle around its surface normal for the excitation photon energy at $\hbar\omega=2.33\text{eV}$ [14]. From this analysis we have concluded that the observed SH light is generated mainly from the electric dipole polarization within a few atomic layers from the $\text{H}_2\text{O}/\text{rutile TiO}_2(110)$ interface. The contribution of the bulk higher order electromagnetic multipoles turned out to be not so large. We have also found that the SH intensity pattern drastically changed as the photon energy was changed [14][19]. We suggested in the paper that the anisotropy of SH radiation is related to the anisotropy of the Ti-O-Ti-O- chains on the $\text{TiO}_2(110)$ surface (Fig. 1).

In the present work we measured SH intensity spectra from the rutile $\text{TiO}_2(110)$ face for various polarization configurations and sample rotation angle around its surface normal. In order to discuss the physical meaning of the spectra, we combined the analysis of the SH intensity spectra

with that of the SH intensity patterns. We first performed analyses of the SH intensity patterns by a phenomenological theory at several photon energies. For this purpose we also needed the data from the $\text{TiO}_2(001)$ face for comparison. We fitted the theoretical SH intensity patterns to the observed ones of the (110) and (001) faces simultaneously. Between the $\text{TiO}_2(110)$ and (001) faces, the surface nonlinear susceptibilities are different but the bulk nonlinear susceptibility is common. For the analysis of the (001) face we also needed the incidence angle dependence of the SH intensity in order to remove the uncertainty in the fitting process. Then we gave an interpretation to the SH intensity spectra taking account of the obtained dominant susceptibility elements.

From the analysis of the SH intensity patterns and spectra it became clear that the surface Ti-O-Ti-O- chains contribute dominantly to the anisotropic SH radiation. In order to confirm the validity of this model and to establish the strong way to analyze the SH response of the crystal surface in general, we have performed an *ab initio* calculation of the electronic states of the $\text{TiO}_2(110)$ surface and have calculated its SH intensity spectra and patterns [20].

This paper is organized as follows. In section 2 we show first the method of our sample preparation, our experimental setup for the SH spectroscopy, and the methods of our phenomenological and *ab initio* theoretical analyses. In section 3 we show our experimental results of the SH intensity patterns and spectra of the $\text{TiO}_2(110)$ and (001) faces. In section 4 we show the results of our numerical analysis using the phenomenological theory with nonlinear

susceptibility. In section 5 we show the results of our *ab initio* calculation of the SH intensity. In section 6, we evaluate the results of the phenomenological analysis, discuss the origin of the SHG from the TiO_2 faces, and consider the physical meaning of the observed SH intensity spectra.

2. Experimental

2.1 Sample preparation

The samples were polished rutile $\text{TiO}_2(110)$ and (001) crystal faces (Nakazumi Crystal Laboratory). They were first annealed at 900°C in oxygen atmosphere for 2 hours to remove the bulk oxygen vacancies. Then, they were etched for 2 hours in 5mol/l NaOH aq. solution at about 100°C and subsequently in 2% HF aqueous solution for 1 minute at room temperature, rinsed in pure water and was dried naturally in laboratory. The surface of the $\text{TiO}_2(110)$ face thus prepared was characterized by XPS and RHEED. We could identify a physisorbed H_2O layer on this face and it disappeared after annealing at 370°C in vacuum. We could also see a carbon signal but they were judged to be adsorbed on the H_2O layer. Thus the prepared interface on the $\text{TiO}_2(110)$ bulk can be regarded as a $\text{H}_2\text{O}/\text{TiO}_2(110)$ interface and we call it “the $\text{TiO}_2(110)$ face” in this paper. A RHEED pattern from this (110) face was taken in a vacuum chamber immediately after the chemical etching. They showed distinct (1×1) patterns. Asari et al. have reported two types of (1×2) structures. A RHEED pattern from one of the (1×2) structures looked almost like a (1×1) pattern [21]. Thus, we cannot tell in principle whether the observed (1×1) RHEED patterns from

our sample originate from the (1x1) or (1x2) structures on $\text{TiO}_2(110)$. On the other hand, Onishi et al. have shown by LEED and STM analyses that the (1x1) structure is stable for the annealing temperature lower than 900K while the (1x2) structure is stable for the annealing temperature higher than 1150K [22]. Considering that our chemically etched $\text{TiO}_2(110)$ surface had not experienced a temperature higher than 100°C, the (1x1) surface is more probably realized under the H_2O physisorbed layer. Chung et al also reported that the (110) 1x1 surface is quite inert and the (1x1) structure prepared in UHV remains after exposing it in air for 30 minutes [23]. From these observations we believe that the interface we prepared was $\text{H}_2\text{O}/\text{TiO}_2(110)$ (1x1) [24]. The $\text{TiO}_2(110)$ face thus prepared looked pale yellow and transparent and was expected to have very little oxygen vacancies both in the bulk and at the interface.

"The $\text{TiO}_2(001)$ face" was prepared by the same process as the (110) face. This face is said to reconstruct to form (011) and (114) facets by annealing or to form (1 x 1) surface by fracturing it at room temperature in vacuum [25]. Attempts were not made in the present work to clarify which of the above structures were realized on the prepared $\text{TiO}_2(001)$ face. This is because only the bulk contribution from the (001) face is important from a point of view of determining the nonlinear susceptibility of the (110) face. Surface contribution of the (001) face will become interesting in the future when the surface structures are characterized.

2.2 SHG measurement

The experimental set-up for the SHG measurements used in this study is schematically shown in Fig. 2. The light source of the fundamental frequency is an optical parametric oscillator (OPO) driven by a frequency-tripled Q-switched Nd:YAG laser with light pulses of duration 3ns and repetition rate 10Hz. The pulse energy was 0.5 to 1.0 mJ/pulse. The fundamental light beam from the OPO was passed through a colored glass filter, a polarizer, and a lens and was focused into a spot of 3mm ϕ diameter on the sample surface. The incident angle was 45° from the surface normal. The reflected SH light beam in the specular direction was collected by lenses, passed through a colored glass filter absorbing the fundamental light, a polarizer, lenses, and a monochromator and was detected by a photomultiplier. The signal from the photomultiplier was digitally stored in a personal computer. To compensate for the temporal variation of the incident laser pulse power, we used a reference sample [GaAs(001) in air] and calibrated the signal intensity by taking the ratio of the intensities measured in the signal and reference channels. To compensate for the sensitivity variation of the optical system as a function of the wavelength, the SH intensity of a z-cut wedged quartz (α -SiO₂) plate was measured as a reference. The TiO₂(110), (001) and α -SiO₂ (0001) samples were mounted on a sample stage with a sliding mechanism and their absolute SH intensities were measured in exactly the same optical configuration. For measuring the dependence of the SH intensity on the sample rotation angle around its surface normal, the sample was mounted on an automatic rotation stage with the surface normal set parallel to the rotating axis of the stage. All measurements were performed in air at room temperature.

2.3 Phenomenological analysis of the SH intensity patterns

We used Maxwell's equations with a nonlinear source term and calculated the amplitude of a second harmonic wave in a three-layered model shown in Fig. 3. In this model, Layer 1 is a vacuum layer, Layer 2 is the surface layer with second order optical nonlinearity, and Layer 3 is the bulk layer with a higher order optical nonlinearity. The origin of the second order nonlinearity in Layer 2 is the breaking of symmetry in the direction normal to the surface by the discontinuity, reconstruction, or relaxation on the surface. We have assumed that Layer 2 is a thin layer with a uniform linear and nonlinear optical response. In fact the dielectric structure of the real surface layer is not so simple. The assumption is acceptable because the surface layer in this study is much thinner than the wavelength of light. In such a case the radiation from nonlinear polarizations can be regarded as that from one homogeneous dipole sheet. Layer 3 is the bulk region of a centrosymmetric crystal with D_{4h}^{14} structure of the bulk rutile TiO_2 . It does not have a second order optical nonlinearity within a dipole approximation, but has a higher order optical nonlinearity. Layers 2 and 3 are assumed to have a uniaxial dielectric response. Namely, dielectric function ϵ has anisotropic tensor components. In Model 1 the c-axis in Layer 3 lies in direction 1 and in Model 2 it lies in direction 3.

The second order nonlinear polarization in Layer 2 is defined as

$$P_{S,i}^{(2)} = \sum_{jk} \chi_{ijk}^{(2)} E_j E_k \quad (1)$$

using the phenomenological nonlinear susceptibility element $\chi_{ijk}^{(2)}$. E_j or E_k is the local electric field component of the incident light in Layer 2. Following Guyot-Sionnest et al [26] we further define the surface nonlinear susceptibility in the substrate frame as $\chi_{Sijk}^{(2)}$. $\chi_{Sijk}^{(2)}$ is obtained by integrating $\chi_{ijk}^{(2)}$ over the surface layer (Layer 2) as a function of depth. When some of the suffices of the susceptibility include the coordinate 3, the integrand is divided by the dielectric function for the electric field in direction 3 in Layer 2 at the frequency of the corresponding photons. Here coordinate 3 indicates the direction perpendicular to the surface plane. When we have a uniform linear and nonlinear dielectric response in Layer 2 we will have,

$$\chi_{S333}^{(2)} \equiv \frac{\chi_{333}^{(2)} d}{\epsilon_{33}(2\omega)[\epsilon_{33}(\omega)]^2} \quad (2)$$

$$\chi_{S3ij}^{(2)} \equiv \frac{\chi_{3ij}^{(2)} d}{\epsilon_{33}(2\omega)} \quad (i,j=1,2) \quad (3)$$

$$\chi_{Sij3}^{(2)} \equiv \frac{\chi_{ij3}^{(2)} d}{\epsilon_{33}(\omega)} \quad (i,j=1,2) \quad (4)$$

$$\chi_{Sijk}^{(2)} \equiv \chi_{ijk}^{(2)} d \quad (i,j,k=1,2) \quad (5)$$

Coordinates 1 and 2 refer to the directions within the surface plane. For the (110) face the numbers 1, 2, and 3 represent the $[001]$, $[\bar{1}10]$, and $[\bar{1}\bar{1}0]$ directions, respectively. For the (001) face the numbers 1, 2, and 3 represent the $[100]$, $[0\bar{1}0]$, and $[00\bar{1}]$ directions, respectively.

The bulk nonlinear polarization in Layer 3 is written as

$$P_{bulk,i}^{(2)} = \sum_{jkl} \Gamma_{ijkl} E_j \nabla_k E_l \quad (6),$$

where Γ_{ijkl} is the higher-order nonlinear susceptibility [10]. E_j or E_l is the local electric field component of the incident beam in Layer 3. The suffix i represents the direction of the nonlinear polarization at frequency 2ω and the suffices j and l represent the directions of the incident electric field at frequency ω . They refer to the crystallographic axes x , y , and z in the crystal structure of TiO_2 .

There are five and three independent surface nonlinear susceptibility elements $\chi_{Sijk}^{(2)}$ for the $\text{TiO}_2(110)$ and (001) faces and they are shown later in Figs. 9 and 10, respectively. Here we have assumed that the structure of Layer 2 has C_{2v} and C_{4v} symmetries for the $\text{TiO}_2(110)$ and (001) faces, respectively. Layer 3 consists of the bulk rutile TiO_2 crystal. There are eleven nonzero bulk nonlinear susceptibility elements Γ_{ijkl} according to the symmetry of its crystal structure D_{4h}^{14} and they are shown later in Fig. 11.

In order to calculate the SH intensity, the electric field amplitude of the incident laser beam in Layers 2 and 3 is calculated first using Maxwell's equations as shown in Appendix A-1. Then the nonlinear polarizations in Layers 2 and 3 are obtained by using equations (1) and (6). Finally, the amplitude of the electric field radiated by the nonlinear polarizations (1) and (6) are calculated by Maxwell's equations with nonlinear source terms as,

$$\nabla \times (\nabla \times \vec{E}) + \frac{1}{c^2} \frac{\partial^2 \vec{\epsilon} \vec{E}}{\partial t^2} = -\frac{4\pi}{c^2} \frac{\partial^2 \vec{P}_{NL}}{\partial t^2} \quad (7)$$

as shown in Appendix A-2.

2.4 Method of *ab initio* calculation

The optical second harmonic (SH) response of the rutile $\text{TiO}_2(110)$ surface was further studied by application of the self-consistent full potential linearized augmented plane-wave (FLAPW) method within the local-density approximation. *Ab initio* calculations of the surface SH response was performed for only a few surface systems of metal and elemental semiconductor such as Si [27]. In the case of TiO_2 , there have been a lot of theoretical studies on the electronic states, the linear optical property [28][29], the surface structure, and the surface electronic states [30][31][32][33][34][35], but there has been no calculation for surface SH response.

The details of the *ab initio* calculation will be published elsewhere [20][36]. In short, for modeling the rutile $\text{TiO}_2(110)$ 1×1 surface we applied a repeated slab construction. The structure of the relaxed $\text{TiO}_2(110)$ surface was calculated by using the *ab initio* pseudopotential (PP) method within the generalized gradient approximation (GGA). The calculations of the ground state and the optical properties were made by application of the FLAPW method within the local-density approximation (LDA) of Hedin and Lundqvists [37]. Density, potential, and basis functions inside the atomic spheres were expanded into spherical harmonics up to $l_{\text{max}}=8$. Reciprocal-space integration was performed with the Gaussian smearing technique applying a width of 0.1 eV.

In the standard density-functional theory (DFT) calculation within the LDA, calculated band gaps are typically smaller than the experimental data and give rise to red-shifted calculated

spectra. In order to improve the agreement of the calculation with the experimental data, quasi-particle (QP) corrections have been often used. A scissors-like operator scheme was used for this purpose. The scissors-like operator makes all the unoccupied bands shift upward by a constant energy Δ_{QP} leaving the occupied bands unshifted. In this study the value of $\Delta_{QP}=1.5\text{eV}$ was chosen to match the calculated absorption edge with the measured one.

The second-order nonlinear optical susceptibility tensor $\chi_s^{(2)}$ was calculated referring to the formalism of Ref. [20][36][38][39]. The imaginary part of the surface nonlinear susceptibility is defined by

$$\begin{aligned} \text{Im}[\chi_{ijk}^{(2)}(\omega)] = & \frac{2\pi}{\Omega} \left(\frac{e}{m\omega}\right)^3 \sum_{k \in \text{SBZ}} \left(\sum_{s \in V} \sum_{r \in C} \sum_{n \in C} \left(\frac{\tilde{p}_{sn}^i \{p_{nr}^j, p_{rs}^k\}}{E_{ns} - 2E_{rs}} [\delta(E_{rs} - \hbar\omega) - 2\delta(E_{ns} - 2\hbar\omega)] \right. \right. \\ & \left. \left. + \frac{\tilde{p}_{nr}^i \{p_{rs}^k, p_{sn}^j\}}{E_{ns} + E_{rs}} \delta(E_{rs} - \hbar\omega) \right) \right. \\ & \left. - \sum_{s \in V} \sum_{l \in V} \sum_{n \in C} \left(\frac{\tilde{p}_{ln}^i \{p_{sl}^j, p_{ns}^k\}}{E_{nl} - 2E_{ns}} [\delta(E_{ns} - \hbar\omega) - 2\delta(E_{nl} - 2\hbar\omega)] \right. \right. \\ & \left. \left. + \frac{\tilde{p}_{sl}^i \{p_{ns}^k, p_{ln}^j\}}{E_{ns} + E_{nl}} \delta(E_{ns} - \hbar\omega) \right) \right) \end{aligned} \quad (8)$$

where the braces indicate a symmetrization of the components j and k , Ω is the volume of the slab in the unit cell, e and m are the electronic charge and mass, and ω denotes the frequency of the incident photon. The notations s , r , n , and l indicate electronic states of the valence (V) or conduction (C) bands. E_{ns} denotes the direct energy gap between the one electron energy levels n and s . The symbol $p_{nr}^j(k)$ denotes the matrix element of the momentum operator \vec{p} defined by $p_{nr}^j = -i\hbar \langle \Psi_n(k) | \nabla_j | \Psi_r(k) \rangle$. The symbol $\tilde{p}_{nr}^i(k)$ marks the matrix element of the modified

momentum operator for the emission of SH radiation defined by $\tilde{p} = \frac{1}{2}[S(z)\hat{p} + \hat{p}S(z)]$, where $S(z)$ is a function which decays inside the slab. In order to obtain the real part of the optical susceptibility, the Kramers-Kronig transformation was used. Using the nonlinear and linear susceptibilities thus obtained, the SH intensity was calculated according to the procedure described in section 2.3.

3. Measured SH intensity from the $\text{TiO}_2(110)$ and (001) faces

3.1 SH intensity patterns from the $\text{TiO}_2(110)$ face

In Fig. 4 we show the SH intensity from the $\text{TiO}_2(110)$ face as a function of the sample rotation angle around its surface normal, for different polarization combinations and for different SH photon energies. In each pattern the SH intensity is plotted in the radial direction. The direction of the incident plane is defined in reference to the $[001]$ axis as shown in Fig. 4*a* and *d*. In each row the SH intensity patterns for four different polarization combinations are shown. As we go down to the lower rows, the SH photon energy $2\eta\omega$ decreases and approaches the bulk band gap of TiO_2 (3.0eV).

We see that the SH intensity shows symmetric patterns as a function of the sample rotation angle for every photon energy and polarization combination. According to the atomic structure of the $\text{TiO}_2(110)$ interface of C_{2v} symmetry, all the SH intensity patterns have two-fold symmetry. In order to check experimentally whether the observed SHG originates from the region within a few

atomic monolayers from the interface or from the bulk, we have deposited SiO_2 of several nanometer thickness on the $\text{TiO}_2(110)$ face and have measured the SH intensity patterns [40]. The observed patterns were different from those from the $\text{TiO}_2(110)$ face, so that we can say that the SH light observed in Fig. 4 originates mainly from the region within a few monolayers from the $\text{TiO}_2(110)$ interface. The pattern in Fig. 4c is especially sensitive to the SiO_2 deposition and is rotated by 90° degrees by the deposition of SiO_2 layers.

Let us first look at the SH intensity pattern for p-polarized input and p-polarized output (Pin/Pout) light waves at the SH photon energy of $2\eta\omega=4.66\text{eV}$ in Fig. 4a. We see that the SH intensity is higher when the incident plane is parallel to the $[001]$ direction. In this configuration the incident electric field is in the plane containing the Ti-O-Ti-O- chains including the bridging oxygen atoms at the interface (Fig. 1).

Let us turn to the SH intensity patterns for the other polarization combinations in the first row (Fig. 4b, c, and d). In Pin/Sout (Fig. 4b) and Sin/Pout (Fig. 4c) polarization combinations, the SH intensity is weak but we see anisotropic SH intensity patterns clearly. For Sin/Sout polarization combination (Fig. 4d), the SH intensity is as low as the noise level.

We now turn to the SH intensity patterns for SH photon energies other than $2\eta\omega=4.66\text{eV}$. When the SH photon energy $2\eta\omega$ approaches that of the band gap of TiO_2 (3.0eV)[41], the SH intensity becomes weaker and the SH intensity patterns change. All the patterns for Pin/Pout polarization combinations (Fig. 2 a, e, i, and m) consist of two lobes, but at $2\eta\omega=3.65\text{eV}$ the

two-lobed pattern is narrow in the middle ($\phi = 90^\circ$ and 270°). For Pin/Sout polarization combination, the SH intensity has four lobes at all the SH photon energies. For Sin/Pout polarization combination, the SH intensity is large when the incident plane is parallel to the $[1\bar{1}0]$ direction at $2\eta\omega = 4.66\text{eV}$ and 3.65eV , while it is large when the incident plane is parallel to the $[001]$ direction at $2\eta\omega = 4.00\text{eV}$. At the photon energy of $2\eta\omega = 3.34\text{eV}$, the SH intensity is weak and we cannot find a pattern. For Sin/Sout polarization combination, the signal at all the SH photon energies is below or comparable to the noise level.

The variation of the SH intensity patterns should reflect the variation of the shapes of the resonant surface electronic wave functions as a function of the photon energy, because the shapes of the electronic wave function determines the ratio of the magnitudes of nonlinear susceptibility elements. The variation of the absolute SH intensity as a function of the photon energy will be shown in the SH intensity curves later in Fig. 7, at various combination of polarizations and sample rotation angle ϕ , indicated by alphabet from *a* to *e* in small circles in Fig. 4*a*, *b*, and *c*.

3.2 SH intensity patterns from the $\text{TiO}_2(001)$ face

In Fig. 5 we show the SH intensity patterns from the $\text{TiO}_2(001)$ face as a function of the sample rotation angle. For all the four SH photon energies, the SH intensity is large for Pin/Pout polarization combination, is non-zero for Sin/Pout polarization combination, and is at a noise level for the other two polarization combinations. For Pin/Pout polarization combination the SH

response is almost isotropic as a function of the sample rotation angle, but four-fold symmetric component is seen for $2\eta\omega=4.00, 3.65$, and 3.34 eV as shown in Fig. 5*e, i*, and *m*. The ratios of the maximum SH intensities for Pin/Pout polarization combination from the $\text{TiO}_2(110)$ face to those from the $\text{TiO}_2(001)$ face are listed in Table I.

Figure 6 shows the SH intensity from the $\text{TiO}_2(001)$ face as a function of the incident angle for the SH photon energy $2\eta\omega=4.66$ eV. These data are necessary in order to determine whether the surface or bulk contribution is dominant for the (001) face. In Fig. 6 dots with error bars represent SH intensity from the $\text{TiO}_2(001)$ face divided by the SH intensity from the GaAs(001) as a function of the incident angle. The solid curves are calculated SH intensity for selected nonlinear susceptibility elements and will be described in detail later.

3.3 SH intensity from the $\text{TiO}_2(110)$ and $\text{TiO}_2(001)$ faces as a function of the photon energy

In Fig. 7 we show the SH intensity from the $\text{TiO}_2(110)$ face as a function of the SH photon energy $2\eta\omega$ for various polarization combinations and sample rotation angles ϕ . The polarization combination and the sample rotation angle adopted for each panel was indicated in Fig. 4 using the alphabet from *a* to *e* in circles. For example, the polarization combination and the sample rotation angle indicated by the symbol © in Fig. 4*a* gives the SH intensity spectrum in Fig. 7*c* as a function of the SH photon energy. The SH intensity between the photon energies $2\eta\omega=3.36$ eV and 3.64 eV was not measured because the light source we used, *i. e.* the optical parametric oscillator, does not

oscillate in this photon energy region.

In all the five spectra SH intensity rises above the SH photon energy 3eV, but the detailed onset energies of the SH intensity are different between the spectra. In Fig. 7*a* and *c* the onset energy is around 3.2eV. In Fig. 7*b*, *d*, and *e* the SH intensity is weak below $2\eta\omega=3.4\text{eV}$ and rises above this SH photon energy. This is consistent with the fact that Fig. 4*m* for $2\eta\omega=3.34\text{eV}$ exhibits finite SH intensity while Fig. 4*n* and *o* show very weak SH intensities. In Fig. 7*c* we find that SH intensity is almost zero around $2\eta\omega=3.65\text{eV}$ for Pin/Pout polarization combination and at $\phi=90^\circ$. This is consistent with the fact that SH intensity is almost zero at $\phi=90^\circ$ and 270° in Fig. 4*i*. In Fig. 7*d* we find that SH intensity is lower around 4.1eV than at 3.6eV and 4.7eV, while it is higher in Fig. 7*e*. This is consistent with the fact that the SH intensity is higher at $\phi=90^\circ$ in Fig. 4*c* and *k*, while it is higher at $\phi=0^\circ$ in Fig. 4*g*.

In Fig. 8 we show the SH intensity from the $\text{TiO}_2(001)$ face as a function of the SH photon energy $2\eta\omega$ for Pin/Pout polarization combination and with the incident plane parallel to the [100] direction. We see that the SH intensity rises above the photon energy of $2\eta\omega\sim 3.0\text{ eV}$. The SH intensity at 3.65 eV is roughly the maximum intensity in the spectra. This is in contrast to the fact that in Fig. 7*a* and *c* the SH intensity for Pin/Pout polarization combination at $2\eta\omega=3.65\text{eV}$ is far below the maximum intensity in the spectra.

In order to check whether the signal observed in Figs. 7 and 8 is in one- or two-photon resonance with the surface electronic levels, we have measured sum frequency generation from the

TiO₂(110) and TiO₂(001) faces (not shown). The results showed that all the signals were in two photon resonance.

4. Results of the phenomenological analysis of the SH intensity patterns at $2\eta\omega=4.66\text{eV}$

In this section we will carry out a numerical analysis of the observed SH intensity patterns from the TiO₂(110) and TiO₂(001) faces shown in Figs. 4 and 5 by a phenomenological electromagnetic theory using the second order nonlinear optical susceptibilities as adjustable parameters.

Figures 9 and 10 show the calculated SH intensity patterns and the peak intensities from the dielectric structures of Models 1 and 2 illustrated in Fig. 3 for the TiO₂(110) and (001) faces, respectively, when one of the five and three surface nonlinear susceptibility elements $\chi_{Sijk}^{(2)(110)}$ and $\chi_{Sijk}^{(2)(001)}$ are set equal to a common value and the other elements are all set equal to zero. Here, $\chi_{Sijk}^{(2)(110)}$ and $\chi_{Sijk}^{(2)(001)}$ are defined as the surface nonlinear susceptibility for the (110) and (001) faces, respectively. We used dielectric constants of TiO₂, $\epsilon_{//}(2.33\text{eV})=8.821$ and $\epsilon_{//}(4.66\text{eV})=-7.409+i13.24$ for the electric fields parallel to the [001] crystal axis, and $\epsilon_{\perp}(2.33\text{eV})=7.129$ and $\epsilon_{\perp}(4.66\text{eV})=3.165+i8.15$ for the electric fields perpendicular to the [001] axis [42]. The patterns were calculated for all the four combinations of the p- and s-polarized incidence and output. Figs. 11 show the calculated SH intensity patterns and the peak intensities from the dielectric structures of Models 1 and 2, when one of the eleven Γ_{ijkl} elements is set equal to a common value and the other elements are all set equal to zero.

Now we fit the theoretical SH intensity patterns to those obtained in the experiment shown in Figs. 4 and 5. We calculated the linear combinations of the patterns in Figs. 9, 10, and 11 in the complex plane with each pattern multiplied by the relevant nonlinear susceptibility element $\chi_{S,ijk}^{(2)(110)}$, $\chi_{S,ijk}^{(2)(001)}$, or Γ_{ijkl} and then vary the nonlinear susceptibility elements as adjustable parameters. Generally in fortunate cases, we can determine the nonlinear susceptibility elements from the best fit results of this fitting. However, since there are susceptibility elements giving similar patterns as seen in Figs. 9, 10 and 11, we cannot determine the unique set of susceptibility elements. Thus, there is a considerable amount of arbitrariness in the determination of the set of the nonlinear susceptibility elements for these faces and in such a case the fitting program shows unstable output.

In order to overcome this problem we should get further information from other index faces or the incident angle dependence of the SH intensity of the faces under study, in order to get the information of the dominant susceptibility elements [43]. In the present case, we measured the incident angle dependence of the SH intensity from the $\text{TiO}_2(001)$ face as in Fig. 6 and determined whether the surface or bulk contribution is dominant in the SH radiation from the (001) face. We also reduced the number of adjustable susceptibility elements by making groups of the elements giving the same or similar SH intensity patterns, and by making only one member in each group an adjustable parameter in the fitting.

In Fig. 6 the SH intensity was measured relative to the bulk SH intensity from $\text{GaAs}(100)$.

We also show by solid curves the calculated SH intensity by selected nonlinear susceptibility elements from the structure Model 2 divided by the calculated SH intensity from GaAs(100). The nonlinear susceptibility elements considered are $\chi_{S,113}^{(2)(001)}$, $\chi_{S,333}^{(2)(001)}$, and Γ_{yyzz} . The reason why we consider only the element Γ_{yyzz} among the Γ_{ijkl} 's is as follows. In Fig. 11 the bulk nonlinear susceptibility elements giving intense isotropic SH intensity patterns from the (001) face for Pin/Pout polarization combination like that in Fig. 5a is Γ_{yyzz} , Γ_{yzyy} , and Γ_{zyzy} . Among these three elements Γ_{zyzy} does not make dominant contribution in Fig. 5a because the observed SH intensity in Fig. 5c is not so large compared with that in Fig. 5a unlike the corresponding patterns for Γ_{zyzy} in Fig. 11. Γ_{yzyy} gives the same patterns as Γ_{yyzz} , as is shown in Fig. 11 and also as is described later in Eq. (10). Thus we should only consider the Γ_{yyzz} element among the Γ_{ijkl} 's. Comparing the theoretical and experimental data in Fig. 6, it is clear that the $\chi_{S,333}^{(2)(001)}$ element is the most dominant among the three susceptibility elements.

In order to reduce the number of the susceptibility elements, the following non-zero susceptibility elements are selected from the groups of the elements in the parentheses as,

$$\Gamma_{zyyz} (\Gamma_{zyyz}, \Gamma_{zzyy}, \Gamma_{zzzz}) \quad (9)$$

$$\Gamma_{yyzz} (\Gamma_{yyzz}, \Gamma_{yzyy}) \quad (10),$$

and

$$\Gamma_{xxyy} (\Gamma_{xxyy}, \Gamma_{xyyx}) \quad (11).$$

In the present study we further assumed

$$\chi_{S113}^{(2)(001)} = 0, \quad \Gamma_{zyzy} = 0 \quad (12)$$

from the above discussion on Fig. 6. We also assumed

$$\Gamma_{yzyz} = 0 \quad (13)$$

because we have found that the SH intensity in Fig. 4c is not due to the bulk response as was mentioned in section 3.1.

In Fig. 12 we show the calculated SH intensity patterns fitted to the experimental data. The patterns in Fig. 12 *a* to *d* reproduce the measured patterns in Fig. 4 *a* to *d*, while patterns in Fig. 12 *e* to *h* reproduce the measured ones in Fig. 5 *a* to *d*. We find that the calculation based on the phenomenological theory reproduces the experimental data very well. In Fig. 13, the calculated patterns in Fig. 12 *a* to *d* are decomposed into the surface (*a* to *d*) and bulk (*e* to *h*) contributions. In the SH intensity patterns for all the polarization combinations except Sin/Sout, the surface contribution is dominant.

Further separating the calculated SH intensity patterns for Pin/Pout polarization combination at $2\eta\omega=4.66\text{eV}$ into the contribution of each susceptibility element, we find that the contribution of the $\chi_{S113}^{(2)(110)}$ element is the largest and then the $\chi_{S223}^{(2)(110)}$ and $\chi_{S333}^{(2)(110)}$ elements are the next largest in the SH intensity. To the SH intensity for Pin/Sout polarization combination the $\chi_{S113}^{(2)(110)}$ and $\chi_{S223}^{(2)(110)}$ elements contribute. For Sin/Pout polarization combination the $\chi_{S311}^{(2)(110)}$ and $\chi_{S322}^{(2)(110)}$ elements contribute much, but the resulting SH intensity pattern is determined as a result of the interference between many susceptibility elements, so it is not easy to

determine which elements dominate the observed SH intensity pattern. For Sin/Sout polarization combination the bulk contribution (Fig. 13*h*) is larger than that from the surface (Fig. 13*d*), but this is a result of erroneous separation of the noise component.

Most of the signals from the TiO₂(001) face for Pin/Pout polarization combination is assigned to the surface contribution, and the $\chi_{s333}^{(2)(001)}$ element was shown to contribute most dominantly to the SH intensity (not shown). This is consistent with the result in Fig. 6.

The SH intensity pattern in Fig. 5*c* is reproduced as a four-fold symmetric curve as shown in Fig. 12*g*. The four-fold symmetric component is attributed to the bulk higher-order nonlinearity, because we see in Fig. 10 that no surface component gives a four-fold symmetric pattern. The four-fold symmetric component for Sin/Pout polarization combination is mostly given by the Γ_{xxxx} and Γ_{xxyy} elements, while the isotropic component is given by the $\chi_{s311}^{(2)(001)}$ element.

The analysis of the SH intensity patterns in Figs. 4 and 5 for the SH photon energies $2\eta\omega=4.00$ and 3.65eV gave similar results, and the dominant contribution of SH intensity from the TiO₂(110) face for the Pin/Pout polarization combination came from the $\chi_{s113}^{(2)(110)}$ element. The dependence of the SH intensity pattern on the photon energy as seen in Fig. 4*c*, *g*, and *k* is very interesting, but we could not determine from this analysis which nonlinear susceptibility element is responsible for this pattern variation because many susceptibility elements contribute to the SH intensity for this polarization combination. The dominant susceptibility element will be analyzed in a qualitative discussion in section 6.3.

At $2\eta\omega=3.34\text{eV}$ the fitting error was so large and we could not determine whether surface or bulk contribution was dominant. Since the SH intensity patterns in Fig. 5 shows four-fold symmetric component for the Pin/Pout polarization combination for the lower photon energies, the bulk contribution is judged to be stronger for the lower photon energies.

5. Results of the *ab initio* calculation

Here we show the results of our recent *ab initio* calculation according to the procedure described in section 2.4 of the SH intensity from the $\text{TiO}_2(110)$ surface and will compare the results with our experiment. Further details can be found in our future publication [20].

Firstly, we note that in the calculated density of states (DOS) of the relaxed surface two peaks assigned to the bridging oxygen $\alpha\text{-O}$ in Fig. 1 were seen at the top of the valence band and around the energy of -16eV (not shown). The DOS of $\alpha\text{-O}$ has a peak at the energy of $\sim 1\text{eV}$ below the top of the valence band for the relaxed surface, while it was found just at the top of the valence band for the unrelaxed surface. This peak shift indicates that the surface relaxation reduces the energy of the electronic state of $\alpha\text{-O}$. Because the valence band of TiO_2 consists of the filled states of oxygen atoms, this reduction of the energy of $\alpha\text{-O}$ gives rise to a larger surface band gap energy than that of the bulk.

Five nonlinear optical susceptibility elements $\chi_{S113}^{(2)(110)}$, $\chi_{S223}^{(2)(110)}$, $\chi_{S311}^{(2)(110)}$, $\chi_{S322}^{(2)(110)}$, and $\chi_{S333}^{(2)(110)}$ were calculated from the wave functions of the $\text{TiO}_2(110)$ surface by the *ab initio*

calculation. The other components were zero due to the symmetry selection rules of the $\text{TiO}_2(110)$ 1×1 surface. Using these nonlinear and also linear optical susceptibility we have calculated SH intensity as shown in Figs. 14 and 15.

The measured SH intensity for Pin/Pout polarization combination and for $k_{\parallel}/[001]$ shown as empty circles in Fig. 14 is much larger than that for Sin/Pout polarization combination and for $k_{\parallel}/[001]$ shown as gray filled circles. The measured SH intensity for the two configurations increases sharply around the SH photon energy of $2\eta\omega=3.5\text{eV}$. These features are mostly reproduced by the calculated SH intensity of the relaxed $\text{TiO}_2(110)$ surface by a solid curve for Pin/Pout polarization combination and by a dashed curve for Sin/Pout polarization combination. However, we also notice that the experiment for the Pin/Pout polarization combination shows a gradual rise in SH intensity at lower energy than the calculation.

Figure 15 shows the calculated SH intensity patterns as a function of the sample rotation angle around the surface normal at the SH photon energy $2\eta\omega=4.0\text{ eV}$. The calculated results of the relaxed surface agree well with the experimental data in Fig. 4e to h from the view points of both the shapes of angle patterns and the intensity ratios between different polarization combinations. Here we note that the calculated results of the unrelaxed surface did not reproduce the measured data at all.

We have also examined which of the Ti-O pairs on the $\text{TiO}_2(110)$ surface dominantly contribute to the SH response. As shown in Fig. 1, the top surface of rutile $\text{TiO}_2(110)$ consists of

four atomic species, *i. e.* bridging oxygen (α), in-plane oxygen (β), 6-fold coordinated titanium (γ), and 5-fold coordinated titanium (δ). Accordingly, there are three pairs of Ti and O atoms adjacent to each other: α -O- γ -Ti, β -O- γ -Ti, and β -O- δ -Ti. We calculated SH response from electronic wave functions localized in each Ti-O pair. We found that the calculated pattern of the α -O- γ -Ti pair agreed with the measured pattern, while the other two calculated patterns did not. Furthermore, calculated SH intensity of the α -O- γ -Ti pair was more than a few hundreds times larger than those of the other pairs. Therefore, most of the SH intensity in Pin/Pout polarization combination is judged to come from the α -O- γ -Ti pairs.

The fact that the calculated SH intensity patterns correctly predicted the experimental results means that not only the absolute value of the surface nonlinear susceptibility but also its phase has been calculated properly. This in turn indicates that the wave functions of the electrons at the $\text{TiO}_2(110)$ surface has been calculated sufficiently well for the purposes of this study.

6. Discussion

6.1 Evaluation of the phenomenological analysis

The phenomenological analysis does not give a physical insight into the origin of the SH intensity, but clarifies dominant nonlinear susceptibility elements, and thus helps us to interpret the SH intensity spectra. The simultaneous numerical analysis of the (110) and (001) faces in the present study gives us the nonlinear susceptibility elements with less ambiguity than separate analyses for

the two faces [14][43]. However, there was still some arbitrariness in the obtained set of nonlinear susceptibility elements and we had to make several assumptions to get the susceptibility elements for physical discussion.

Nevertheless, the analysis at the SH photon energy of $2\eta\omega=4.66\text{eV}$ was quite successful. This fact indicates that also at other photon energies such as at $2\eta\omega=3.34\text{eV}$ we can determine nonlinear susceptibility if we could measure SH intensity patterns with better S/N ratio. In this work we used tunable nanosecond optical pulses, but if we could use picosecond pulses, the SH response would be stronger. Then we could even perform real time determination of the nonlinear susceptibility elements, while we scan the wavelength of the tunable light source, just as we do in the spectroscopic ellipsometry experiment.

It is very interesting that the higher-order bulk optical nonlinearity was observed through the four-fold symmetric component in the SH intensity patterns for Pin/Pout and Sin/Pout polarization combination in Fig. 5. However, the four-fold symmetric component in the SH intensity patterns do not dominate the signal intensity, and we cannot get detailed information from the present result.

6.2 Origin of the SHG from the $\text{TiO}_2(110)$ face

One of the biggest findings in this study is that strong SH response to the electric field parallel to the [001] direction has been assigned to the surface contribution. From this fact and the

discussion below we think that the SH intensity for this (110) face stems mainly from the Ti-O-Ti-O- chains on this surface.

Goniakowski and Gillan [44] has predicted that the surface bridging oxygen state is located at the top of the bulk valence band in the energy band diagram. This leads us to think that the observed upward two photon transition may start from the bridging oxygen state because the SH photon energy in the present study is just above the bulk band gap energy of TiO_2 . Then the electron will be successively excited by two photons of the same photon energy and reach the empty Ti state. These electronic transitions correspond to the electron movement from the α -O to γ -Ti in Fig. 1, *i. e.* within the Ti-O-Ti-O chains. This picture is also supported by the fact that in Fig. 4a the SH intensity from the $\text{TiO}_2(110)$ face for Pin/Pout polarization combination is large at the sample rotation angle $\phi=0^\circ$. At this sample rotation angle the incident electric field is parallel to the Ti-O-Ti-O- chain and thus the movement of the electron is induced within the chain. It has been generally pointed out that the Ti-O-Ti-O- chain is very important in designing the nonlinear optical materials [45].

It is also interesting to find that the *ab initio* calculation at $2\eta\omega=4.0\text{eV}$ supports this model of resonant SH photon emission from the Ti-O-Ti-O- chains consisting of α -O- γ -Ti pairs. Generally, we must be careful in adopting the results of theoretical calculations. However, in this study the *ab initio* calculation reproduces the experimental SH intensity patterns and spectra to a considerable extent. In such a case we feel that the *ab initio* calculation is quite reliable in

predicting various linear and nonlinear optical properties of this surface. Though Ti and O atoms below the top surface also contribute to the total surface SH response, their contribution drastically decreases as they go deep into the bulk. Therefore, we conclude that the Ti-O-Ti-O- zigzag chains consisting of α -O and γ -Ti on the top surface dominantly contribute to the SH response of the $\text{TiO}_2(110)$ surface.

6.3 SH intensity spectra of the Ti-O-Ti-O- chain

In this section we discuss the electronic states of the surface Ti-O-Ti-O- chain from the observed SH intensity spectra in Fig. 7. The electronic states we discuss in this photon energy region have not been treated well by photoemission or inverse photoemission spectroscopy [46][47][48].

In order to analyze the SH intensity spectra we further discuss the nonlinear susceptibility elements responsible for the SH intensity patterns in Fig. 4. In the SH intensity pattern analysis in section 4 we could not deduce which nonlinear susceptibility element is responsible for the variation of the SH intensity patterns for Sin/Pout polarization combination in Fig. 4*c*, *g*, and *k*. However, judging from the result of a separate experiment in section 3.1 that the SH intensity patterns for Sin/Pout polarization combination are sensitive to the additive deposition of SiO_2 layers, we can say that the signals in this polarization combination comes mainly from the surface. Then from the calculated patterns in Fig. 9, we can say that the patterns for the Sin/Pout polarization combination in Fig. 2*c* and *k* are dominated by the nonlinear susceptibility element $\chi_{S311}^{(2)(110)}$, and

that in Fig. 2g is dominated by $\chi_{S322}^{(2)(110)}$.

For the discussion of the electronic states, we first note that the onset energy of the rise of the SH intensity is different between Fig. 7a, d, and e. In the spectra in Fig. 7a, d, and e, the dominant susceptibility element is suggested to be $\chi_{S113}^{(2)(110)}$, $\chi_{S311}^{(2)(110)}$, and $\chi_{S322}^{(2)(110)}$, respectively, from the above discussion. In Fig. 7a the onset energy is around 3.2eV, while in Fig. 7d and e it is around 3.4eV. The observed difference in the photon energy of the SH intensity rise between Fig. 2a, d and e should reflect the difference in the electronic states or the electronic confinement in the Ti-O-Ti-O- zigzag chain. Here we model the Ti-O-Ti-O- zigzag chain as a quantum wire and consider the behavior of the electron in this wire. In the second harmonic generation process described by the nonlinear susceptibility element of $\chi_{S113}^{(2)(110)}$ dominating the SH intensity in Fig. 7a, the final transition dipole with frequency 2ω is induced in direction 1. In the second harmonic generation process described by the nonlinear susceptibility elements of $\chi_{S311}^{(2)(110)}$ and $\chi_{S322}^{(2)(110)}$ dominating the SH intensity in Fig. 7d and e, respectively, the final transition dipole with frequency 2ω is induced in direction 3. The electronic wave function in the Ti-O-Ti-O- chain is delocalized in the direction of the chain axis (direction 1) but localized in the direction perpendicular to the chain axis (direction 3). Thus the transition energy should be smaller in the process described by $\chi_{S113}^{(2)(110)}$ as in Fig. 7a and larger in the process described by $\chi_{S311}^{(2)(110)}$ and $\chi_{S322}^{(2)(110)}$ as in Fig. 7d and e. However, this feature is not seen in the calculated results by the *ab initio* method in Fig. 14. The clarification of this discrepancy will be our future problem.

It is also interesting to note that the spectra in Fig. 7d is the up-side-down image of the one in Fig. 7e in the photon energy region from 3.6eV to 4.8eV. This feature is consistent with the observed patterns in Fig. 4c, g, and k. Namely, in these patterns the SH intensity is strong either at $\phi=0$ or 90° exclusively. This may be one feature of the energy spectrum of the electrons confined in a quantum wire. Namely, different modes of electronic oscillation may be exhibited in these two spectra. However, the check of the validity of this guess will also be our future problem.

It is also interesting that the SH intensity spectrum of the $\text{TiO}_2(001)$ face in Fig. 8 exhibits a lower onset energy of the SH intensity rise than any of the spectra in Fig. 7. As is pointed out in section 2.1, the structure of the $\text{TiO}_2(001)$ face is not characterized in this study so that we have no idea about the origin of this difference. However, we can say at least that the $\text{TiO}_2(001)$ face has an interface electronic state different from that of the $\text{TiO}_2(110)$ face.

7. Conclusion

We have observed optical second harmonic generation (SHG) from the rutile $\text{H}_2\text{O}/\text{TiO}_2(110)$ and (001) interfaces as a function of the sample rotation angle ϕ around its surface normal and the polarizations of incident and second harmonic light at different SH photon energies. Anisotropy in the nonlinear optical response from its surface and bulk depended strongly on the SH photon energy. In order to separate the contributions from various nonlinear susceptibility elements we have performed a numerical analysis of the SH intensity patterns as a function of ϕ

from the $\text{TiO}_2(110)$ and (001) faces simultaneously. We have found that the surface contribution is dominant at most of the measured photon energies and the most dominant contribution in P-in/P-out polarization combination was the $\chi_{s113}^{(2)(110)}$ element. We have also obtained SH intensity spectra from the $\text{TiO}_2(110)$ and (001) faces as a function of the SH photon energy. For interpreting these SH intensity spectra the results of the SH intensity pattern analyses were used. We have found that the onset of the SH resonance of the $\text{TiO}_2(110)$ interface is $2\eta\omega \sim 3.4\text{eV}$ with the nonlinear polarization at $2\eta\omega$ perpendicular to the surface, while it is $2\eta\omega \sim 3.2\text{eV}$ with the nonlinear polarization at $2\eta\omega$ parallel to the $[001]$ direction in the surface plane. *Ab initio* calculation by using the FLAPW method within the local-density approximation is shown to predict correctly the SH intensity patterns and spectra. The result that the SH intensity patterns were predicted fairly well indicates that the wave functions of the surface have been calculated sufficiently well for optical application. Also by using the calculated results, Ti-O-Ti-O- chains including the bridging oxygen atoms on the surface has been identified as the main origin of the SH radiation from the $\text{TiO}_2(110)$ surface.

Summarizing all these results, titanium dioxide has turned out to be a very good example for a consistent investigation of experiment, phenomenological theory and *ab initio* calculation of surface second harmonic radiation. The findings made in this paper will further give a progress in studying the mechanisms of the photocatalytic, superhydrophilic, and biocompatible properties of this material.

Appendix

In this appendix we review a theoretical treatment of the reflected SH radiation from an anisotropic medium like rutile TiO₂. Similar treatment was shown by several authors [13][14]. So we only show the equations used in our calculation.

A-1 Linear reflection and refraction in an anisotropic medium

First, we show the equation for the internal field of the excitation beam in a dielectric structure in

Fig. 3.

For the (110) face (Model 1) it is,

$$\begin{pmatrix}
 -\sin\phi & -\cos\theta\cos\phi & -e_{2o\downarrow x}^\omega & -e_{2e\downarrow x}^\omega & -e_{2o\uparrow x}^\omega & -e_{2e\uparrow x}^\omega & 0 & 0 \\
 \cos\phi & -\cos\theta\sin\phi & -e_{2o\downarrow y}^\omega & -e_{2e\downarrow y}^\omega & -e_{2o\uparrow y}^\omega & -e_{2e\uparrow y}^\omega & 0 & 0 \\
 \cos\theta\cos\phi & -\sin\phi & -a_{2o\downarrow x}^\omega & -a_{2e\downarrow x}^\omega & -a_{2o\uparrow x}^\omega & -a_{2e\uparrow x}^\omega & 0 & 0 \\
 \cos\theta\sin\phi & \cos\phi & -a_{2o\downarrow y}^\omega & -a_{2e\downarrow y}^\omega & -a_{2o\uparrow y}^\omega & -a_{2e\uparrow y}^\omega & 0 & 0 \\
 0 & 0 & e_{2o\downarrow x}^\omega e^{i\alpha_{2o}^\omega} & e_{2e\downarrow x}^\omega e^{i\alpha_{2e}^\omega} & e_{2o\uparrow x}^\omega e^{-i\alpha_{2o}^\omega} & e_{2e\uparrow x}^\omega e^{-i\alpha_{2e}^\omega} & -e_{3o\downarrow x}^\omega e^{i\alpha_{3o}^\omega} & -e_{3e\downarrow x}^\omega e^{i\alpha_{3e}^\omega} \\
 0 & 0 & e_{2o\downarrow y}^\omega e^{i\alpha_{2o}^\omega} & e_{2e\downarrow y}^\omega e^{i\alpha_{2e}^\omega} & e_{2o\uparrow y}^\omega e^{-i\alpha_{2o}^\omega} & e_{2e\uparrow y}^\omega e^{-i\alpha_{2e}^\omega} & -e_{3o\downarrow y}^\omega e^{i\alpha_{3o}^\omega} & -e_{3e\downarrow y}^\omega e^{i\alpha_{3e}^\omega} \\
 0 & 0 & a_{2o\downarrow x}^\omega e^{i\alpha_{2o}^\omega} & a_{2e\downarrow x}^\omega e^{i\alpha_{2e}^\omega} & a_{2o\uparrow x}^\omega e^{-i\alpha_{2o}^\omega} & a_{2e\uparrow x}^\omega e^{-i\alpha_{2e}^\omega} & -a_{3o\downarrow x}^\omega e^{i\alpha_{3o}^\omega} & -a_{3e\downarrow x}^\omega e^{i\alpha_{3e}^\omega} \\
 0 & 0 & a_{2o\downarrow y}^\omega e^{i\alpha_{2o}^\omega} & a_{2e\downarrow y}^\omega e^{i\alpha_{2e}^\omega} & a_{2o\uparrow y}^\omega e^{-i\alpha_{2o}^\omega} & a_{2e\uparrow y}^\omega e^{-i\alpha_{2e}^\omega} & -a_{3o\downarrow y}^\omega e^{i\alpha_{3o}^\omega} & -a_{3e\downarrow y}^\omega e^{i\alpha_{3e}^\omega}
 \end{pmatrix}
 \begin{pmatrix}
 E_{rs0}^\omega \\
 E_{rp0}^\omega \\
 E_{2o\downarrow 0}^\omega \\
 E_{2e\downarrow 0}^\omega \\
 E_{2o\uparrow 0}^\omega \\
 E_{2e\uparrow 0}^\omega \\
 E_{3o\downarrow 0}^\omega \\
 E_{3e\downarrow 0}^\omega
 \end{pmatrix}
 =
 \begin{pmatrix}
 -\cos\theta\cos\phi E_{inp0}^\omega + \sin\phi E_{ins0}^\omega \\
 -\cos\theta\sin\phi E_{inp0}^\omega - \cos\phi E_{ins0}^\omega \\
 \sin\phi E_{inp0}^\omega + \cos\theta\cos\phi E_{ins0}^\omega \\
 -\cos\phi E_{inp0}^\omega + \cos\theta\sin\phi E_{ins0}^\omega \\
 0 \\
 0 \\
 0 \\
 0
 \end{pmatrix}
 \quad (A.1)$$

where E_{ri0}^ω ($i=s, p$) is the electric field amplitude of the reflected light of i -polarization in Layer 1.

It is defined by

$$\vec{E}_{rs}^\omega = E_{rs0}^\omega \begin{pmatrix} -\sin \phi \\ \cos \phi \\ 0 \end{pmatrix} e^{\frac{i\omega}{c}(\sin \theta \cos \phi x + \sin \theta \sin \phi y - \cos \theta z) - i\omega t} \quad (\text{A.2})$$

$$\vec{E}_{rp}^\omega = E_{rp0}^\omega \begin{pmatrix} -\cos \theta \cos \phi \\ -\cos \theta \sin \phi \\ -\sin \theta \end{pmatrix} e^{\frac{i\omega}{c}(\sin \theta \cos \phi x + \sin \theta \sin \phi y - \cos \theta z) - i\omega t} \quad (\text{A.3})$$

where \vec{E}_{rs}^ω and \vec{E}_{rp}^ω are the s- and p-polarized reflected electric fields, respectively. E_{ijk}^ω ($i=2, 3; j=e, o; k=\downarrow, \uparrow$) is the electric field in the i -th layer and is defined by

$$\vec{E}_{ijk}^\omega = E_{ijk0}^\omega \vec{e}_{ijk}^\omega e^{i\vec{k}_{ijk} \cdot \vec{r} - i\omega t} \quad (\text{A.4})$$

The suffices e and o denote the *extraordinary* and *ordinary* electromagnetic waves, respectively.

The suffices \downarrow and \uparrow denote the downward and upward propagating waves, respectively. The

vector \vec{e}_{ijk}^ω is the unit polarization vector of the electric field and can be written as

$$e_{iok}^\omega = \frac{1}{\sqrt{\epsilon_{i\perp}^\omega - \sin^2 \theta \cos^2 \phi}} \begin{pmatrix} 0 \\ -\sqrt{\epsilon_{i\perp}^\omega - \sin^2 \theta} \\ \pm \sin \theta \sin \phi \end{pmatrix} \quad (\text{A.5})$$

(+ and - signs for $k=\downarrow$ and \uparrow , respectively)

$$e_{iek}^\omega = \frac{1}{\sqrt{\epsilon_{i\parallel}^\omega + \left(\frac{\epsilon_{i\parallel}^\omega}{\epsilon_{i\perp}^\omega}\right) \sin^2 \theta \cos^2 \phi \left(\frac{\epsilon_{i\parallel}^\omega}{\epsilon_{i\perp}^\omega} - 1\right)}}$$

$$\times \begin{pmatrix} \frac{\sqrt{\epsilon_{i//}^\omega (1 - \frac{1}{\epsilon_{i\perp}^\omega} \sin^2 \theta \cos^2 \phi)}}{\epsilon_{i//}^\omega \sin^2 \theta \cos \phi \sin \phi} \\ \frac{\epsilon_{i\perp}^\omega \sin \theta \cos \phi}{\epsilon_{i\perp}^\omega \sqrt{\epsilon_{i//}^\omega (1 - \frac{1}{\epsilon_{i\perp}^\omega} \sin^2 \theta \cos^2 \phi)}} \sqrt{\epsilon_{i//}^\omega - \sin^2 \theta \sin^2 \phi - \frac{\epsilon_{i//}^\omega}{\epsilon_{i\perp}^\omega} \sin^2 \theta \cos^2 \phi} \end{pmatrix} \quad (\text{A.6})$$

(- and + signs for $k=\downarrow$ and \uparrow , respectively)

and \bar{k}_{ijk} in eq. (A.4) is defined by

$$\bar{k}_{iok}^\omega = \frac{\omega}{c} \begin{pmatrix} \sin \theta \cos \phi \\ \sin \theta \sin \phi \\ \pm \sqrt{\epsilon_{i\perp}^\omega - \sin^2 \theta} \end{pmatrix} \quad (\text{A.7})$$

$$\bar{k}_{iek}^\omega = \frac{\omega}{c} \begin{pmatrix} \sin \theta \cos \phi \\ \sin \theta \sin \phi \\ \pm \sqrt{\epsilon_{i//}^\omega - \sin^2 \theta \sin^2 \phi - \frac{\epsilon_{i//}^\omega}{\epsilon_{i\perp}^\omega} \sin^2 \theta \cos^2 \phi} \end{pmatrix} \quad (\text{A.8})$$

(+ and - signs for $k=\downarrow$ and \uparrow , respectively)

a_{ijkx}^ω and $a_{ijk y}^\omega$ in the matrix elements in eq. (A.1) are defined by

$$a_{ijkx}^\omega = \frac{c}{\omega} (k_{ijk y}^\omega e_{ijkz}^\omega - k_{ijkz}^\omega e_{ijk y}^\omega) \quad (\text{A.9})$$

$$a_{ijk y}^\omega = \frac{c}{\omega} (k_{ijkz}^\omega e_{ijkx}^\omega - k_{ijkx}^\omega e_{ijkz}^\omega) \quad (\text{A.10})$$

and α_{ij}^ω is defined by

$$\alpha_{ij}^\omega = k_{ij\downarrow z}^\omega d \quad (i=2,3, j=e,o) \quad (\text{A.11}).$$

For the (001) face (Model 2) we can separate the discussion into those of s- and

p-polarized field. The equation for the internal field is

$$\begin{pmatrix} 1 & -e_{2s\downarrow y}^\omega & -e_{2s\uparrow y}^\omega & 0 \\ \cos\theta & -a_{2s\downarrow x}^\omega & -a_{2s\uparrow x}^\omega & 0 \\ 0 & e_{2s\downarrow y}^\omega e^{ik_{2sz}^\omega d} & e_{2s\uparrow y}^\omega e^{-ik_{2sz}^\omega d} & -e_{3s\downarrow y}^\omega e^{ik_{3sz}^\omega d} \\ 0 & a_{2s\downarrow x}^\omega e^{ik_{2sz}^\omega d} & a_{2s\uparrow x}^\omega e^{-ik_{2sz}^\omega d} & -a_{3s\downarrow x}^\omega e^{ik_{3sz}^\omega d} \end{pmatrix} \begin{pmatrix} E_{rs0}^\omega \\ E_{2s\downarrow 0}^\omega \\ E_{2s\uparrow 0}^\omega \\ E_{3s\downarrow 0}^\omega \end{pmatrix} = \begin{pmatrix} -1 \\ \cos\theta \\ 0 \\ 0 \end{pmatrix} E_{ins0}^\omega \quad (\text{A.12})$$

for s-polarized input. For p-polarized input

$$\begin{pmatrix} -\cos\theta & -e_{2p\downarrow x}^\omega & -e_{2p\uparrow x}^\omega & 0 \\ 1 & -a_{2p\downarrow y}^\omega & -a_{2p\uparrow y}^\omega & 0 \\ 0 & e_{2p\downarrow x}^\omega e^{ik_{2pz}^\omega d} & e_{2p\uparrow x}^\omega e^{-ik_{2pz}^\omega d} & -e_{3p\downarrow x}^\omega e^{ik_{3pz}^\omega d} \\ 0 & a_{2p\downarrow y}^\omega e^{ik_{2pz}^\omega d} & a_{2p\uparrow y}^\omega e^{-ik_{2pz}^\omega d} & -a_{3p\downarrow y}^\omega e^{ik_{3pz}^\omega d} \end{pmatrix} \begin{pmatrix} E_{rp0}^\omega \\ E_{2p\downarrow 0}^\omega \\ E_{2p\uparrow 0}^\omega \\ E_{3p\downarrow 0}^\omega \end{pmatrix} = \begin{pmatrix} -\cos\theta \\ -1 \\ 0 \\ 0 \end{pmatrix} E_{inp0}^\omega. \quad (\text{A.13})$$

Here, E_{ri0}^ω ($i=s, p$) is defined in eqs. (A.2) and (A.3). E_{ijk}^ω ($i=2, 3; j=e, o; k=\downarrow, \uparrow$) is

defined in eq. (A.4). e_{ijk}^ω is defined as

$$e_{isk}^\omega = \begin{pmatrix} 0 \\ 1 \\ 0 \end{pmatrix} \quad (\text{A.14})$$

$$e_{ipk}^\omega = \frac{1}{\sqrt{\varepsilon_{i\perp}^\omega [1 + \sin^2 \theta (\varepsilon_{i\perp}^\omega - \varepsilon_{i\parallel}^\omega)]}} \begin{pmatrix} \sqrt{\varepsilon_{i\perp}^\omega (1 - \frac{\sin^2 \theta}{\varepsilon_{i\parallel}^\omega})} \varepsilon_{i\parallel}^\omega \\ 0 \\ \sin \theta \varepsilon_{i\perp}^\omega \end{pmatrix} \quad (\text{A.15})$$

(i, k)=(2, \downarrow), (2, \uparrow), and (3, \downarrow)

(- and + signs for $k=\downarrow$ and \uparrow , respectively)

and \bar{k}_{ijk}^ω is defined as

$$\vec{k}_{isk}^\omega = \frac{\omega}{c} \begin{pmatrix} \sin \theta \\ 0 \\ \pm \sqrt{\varepsilon_{i\perp}^\omega - \sin^2 \theta} \end{pmatrix} \quad (\text{A.16})$$

$$\vec{k}_{ipk}^\omega = \frac{\omega}{c} \begin{pmatrix} \sin \theta \\ 0 \\ \pm \sqrt{\varepsilon_{i\perp}^\omega (1 - \frac{\sin^2 \theta}{\varepsilon_{i\parallel}^\omega})} \end{pmatrix} \quad (\text{A.17})$$

a_{ijkx}^ω , $a_{ijk y}^\omega$, and α_{ij}^ω are defined by (A.9) to (A.11) with $j = s, p$.

A-2 SH electric field radiated from an anisotropic medium

We assume that the nonlinear polarization \vec{P}_0^{NL} is induced in Layer 2. The SH electric field in the dielectric structure described by Model 1 can be written as,

$$\begin{pmatrix} -\sin \phi & -\cos \theta \cos \phi & -e_{2o\downarrow x}^{2\omega} & -e_{2e\downarrow x}^{2\omega} & -e_{2o\uparrow x}^{2\omega} & -e_{2e\uparrow x}^{2\omega} & 0 & 0 \\ \cos \phi & -\cos \theta \sin \phi & -e_{2o\downarrow y}^{2\omega} & -e_{2e\downarrow y}^{2\omega} & -e_{2o\uparrow y}^{2\omega} & -e_{2e\uparrow y}^{2\omega} & 0 & 0 \\ \cos \theta \cos \phi & -\sin \phi & -a_{2o\downarrow x}^{2\omega} & -a_{2e\downarrow x}^{2\omega} & -a_{2o\uparrow x}^{2\omega} & -a_{2e\uparrow x}^{2\omega} & 0 & 0 \\ \cos \theta \sin \phi & \cos \phi & -a_{2o\downarrow y}^{2\omega} & -a_{2e\downarrow y}^{2\omega} & -a_{2o\uparrow y}^{2\omega} & -a_{2e\uparrow y}^{2\omega} & 0 & 0 \\ 0 & 0 & e_{2o\downarrow x}^{2\omega} e^{i\alpha_{2o}^{2\omega}} & e_{2e\downarrow x}^{2\omega} e^{i\alpha_{2e}^{2\omega}} & e_{2o\uparrow x}^{2\omega} e^{-i\alpha_{2o}^{2\omega}} & e_{2e\uparrow x}^{2\omega} e^{-i\alpha_{2e}^{2\omega}} & -e_{3o\downarrow x}^{2\omega} e^{i\alpha_{3o}^{2\omega}} & -e_{3e\downarrow x}^{2\omega} e^{i\alpha_{3e}^{2\omega}} \\ 0 & 0 & e_{2o\downarrow y}^{2\omega} e^{i\alpha_{2o}^{2\omega}} & e_{2e\downarrow y}^{2\omega} e^{i\alpha_{2e}^{2\omega}} & e_{2o\uparrow y}^{2\omega} e^{-i\alpha_{2o}^{2\omega}} & e_{2e\uparrow y}^{2\omega} e^{-i\alpha_{2e}^{2\omega}} & -e_{3o\downarrow y}^{2\omega} e^{i\alpha_{3o}^{2\omega}} & -e_{3e\downarrow y}^{2\omega} e^{i\alpha_{3e}^{2\omega}} \\ 0 & 0 & a_{2o\downarrow x}^{2\omega} e^{i\alpha_{2o}^{2\omega}} & a_{2e\downarrow x}^{2\omega} e^{i\alpha_{2e}^{2\omega}} & a_{2o\uparrow x}^{2\omega} e^{-i\alpha_{2o}^{2\omega}} & a_{2e\uparrow x}^{2\omega} e^{-i\alpha_{2e}^{2\omega}} & -a_{3o\downarrow x}^{2\omega} e^{i\alpha_{3o}^{2\omega}} & -a_{3e\downarrow x}^{2\omega} e^{i\alpha_{3e}^{2\omega}} \\ 0 & 0 & a_{2o\downarrow y}^{2\omega} e^{i\alpha_{2o}^{2\omega}} & a_{2e\downarrow y}^{2\omega} e^{i\alpha_{2e}^{2\omega}} & a_{2o\uparrow y}^{2\omega} e^{-i\alpha_{2o}^{2\omega}} & a_{2e\uparrow y}^{2\omega} e^{-i\alpha_{2e}^{2\omega}} & -a_{3o\downarrow y}^{2\omega} e^{i\alpha_{3o}^{2\omega}} & -a_{3e\downarrow y}^{2\omega} e^{i\alpha_{3e}^{2\omega}} \end{pmatrix} \begin{pmatrix} E_{rs0}^{2\omega} \\ E_{rp0}^{2\omega} \\ E_{2o\downarrow 0}^{2\omega} \\ E_{2e\downarrow 0}^{2\omega} \\ E_{2o\uparrow 0}^{2\omega} \\ E_{2e\uparrow 0}^{2\omega} \\ E_{3o\downarrow 0}^{2\omega} \\ E_{3e\downarrow 0}^{2\omega} \end{pmatrix} = \begin{pmatrix} E_{IH0x} \\ E_{IH0y} \\ \frac{c}{2\omega} (k_{Sy} E_{IH0z} - k_{Sz} E_{IH0y}) \\ \frac{c}{2\omega} (k_{Sz} E_{IH0x} - k_{Sx} E_{IH0z}) \\ -e^{i\alpha_{IH}} E_{IH0x} \\ -e^{i\alpha_{IH}} E_{IH0y} \\ -\frac{c}{2\omega} (k_{Sy} E_{IH0z} - k_{Sz} E_{IH0y}) e^{i\alpha_{IH}} \\ -\frac{c}{2\omega} (k_{Sz} E_{IH0x} - k_{Sx} E_{IH0z}) e^{i\alpha_{IH}} \end{pmatrix} \quad (\text{A.18})$$

Here, $E_{rj0}^{2\omega}$, $E_{ijk0}^{2\omega}$, $e_{ijk}^{2\omega}$, $\vec{k}_{ijk}^{2\omega}$, $a_{ijkx}^{2\omega}$, $a_{ijk y}^{2\omega}$, and $\alpha_{ij}^{2\omega}$ are defined by eqs. (A.2) to (A.11) with ω

replaced with 2ω . α_{IH} is defined by

$$\alpha_{IH} = k_{Sz}d \quad (\text{A.19})$$

and \vec{E}_{IH0} can be calculated from the equation

$$\begin{pmatrix} (k_{Sy}^2 + k_{Sz}^2) - \frac{4\omega^2}{c^2} \varepsilon_{2//}^{2\omega} & -k_{Sx}k_{Sy} & -k_{Sx}k_{Sz} \\ -k_{Sx}k_{Sy} & (k_{Sx}^2 + k_{Sz}^2) - \frac{4\omega^2}{c^2} \varepsilon_{2\perp}^{2\omega} & -k_{Sy}k_{Sz} \\ -k_{Sx}k_{Sz} & -k_{Sy}k_{Sz} & (k_{Sx}^2 + k_{Sy}^2) - \frac{4\omega^2}{c^2} \varepsilon_{2\perp}^{2\omega} \end{pmatrix} \begin{pmatrix} E_{IH0x} \\ E_{IH0y} \\ E_{IH0z} \end{pmatrix} = \frac{16\pi\omega^2}{c^2} \begin{pmatrix} P_{0x}^{NL} \\ P_{0y}^{NL} \\ P_{0z}^{NL} \end{pmatrix} \quad (\text{A.20})$$

The SH electric field in the dielectric structure described by Model 2 can be written as,

$$\begin{pmatrix} -\cos\theta & -e_{2p\downarrow x}^\omega & -e_{2p\uparrow x}^\omega & 0 \\ 1 & -a_{2p\downarrow y}^\omega & -a_{2p\uparrow y}^\omega & 0 \\ 0 & e_{2p\downarrow x}^\omega e^{ik_{2pz}^\omega d} & e_{2p\uparrow x}^\omega e^{-ik_{2pz}^\omega d} & -e_{3p\downarrow x}^\omega e^{ik_{3pz}^\omega d} \\ 0 & a_{2p\downarrow y}^\omega e^{ik_{2pz}^\omega d} & a_{2p\uparrow y}^\omega e^{-ik_{2pz}^\omega d} & -a_{3p\downarrow y}^\omega e^{ik_{3pz}^\omega d} \end{pmatrix} \begin{pmatrix} E_{rp0}^\omega \\ E_{2p\downarrow 0}^\omega \\ E_{2p\uparrow 0}^\omega \\ E_{3p\downarrow 0}^\omega \end{pmatrix} = \begin{pmatrix} E_{IH0x}^{2\omega} \\ H_{IH0y}^{2\omega} \\ -E_{IH0x}^{2\omega} e^{ik_{Sz}d} \\ -H_{IH0y}^{2\omega} e^{ik_{Sz}d} \end{pmatrix} \quad (\text{A.21})$$

for the nonlinear polarization perpendicular to the plane of incidence.

$$\begin{pmatrix} 1 & -e_{2s\downarrow y}^{2\omega} & -e_{2s\uparrow y}^{2\omega} & 0 \\ \cos\theta & -a_{2s\downarrow x}^{2\omega} & -a_{2s\uparrow x}^{2\omega} & 0 \\ 0 & e_{2s\downarrow y}^{2\omega} e^{ik_{2sz}^{2\omega} d} & e_{2s\uparrow y}^{2\omega} e^{-ik_{2sz}^{2\omega} d} & -e_{3s\downarrow y}^{2\omega} e^{ik_{3sz}^{2\omega} d} \\ 0 & a_{2s\downarrow x}^{2\omega} e^{ik_{2sz}^{2\omega} d} & a_{2s\uparrow x}^{2\omega} e^{-ik_{2sz}^{2\omega} d} & -a_{3s\downarrow x}^{2\omega} e^{ik_{3sz}^{2\omega} d} \end{pmatrix} \begin{pmatrix} E_{rs0}^{2\omega} \\ E_{2s\downarrow 0}^{2\omega} \\ E_{2s\uparrow 0}^{2\omega} \\ E_{3s\downarrow 0}^{2\omega} \end{pmatrix} = \begin{pmatrix} E_{IH0y}^{2\omega} \\ H_{IH0x}^{2\omega} \\ E_{IH0y}^{2\omega} e^{ik_{Sz}d} \\ H_{IH0x}^{2\omega} e^{ik_{Sz}d} \end{pmatrix} \quad (\text{A.22})$$

for the nonlinear polarization in the plane of incidence. Here, $E_{rj0}^{2\omega}$ is defined in eqs. (A.2) and

(A.3) with $j = s, p$. $E_{ijk0}^{2\omega}$ is defined in eq. (A.4) with $j = s, p$ and with ω replaced with 2ω . $e_{ijk}^{2\omega}$ is defined in eq. (A.14) and (A.15) with ω replaced with 2ω . $\overline{k}_{ijk}^{2\omega}$ is defined in eq. (A.16) and (A.17) with ω replaced with 2ω . Finally, $a_{ijkx}^{2\omega}$, $a_{ijk y}^{2\omega}$, and $\alpha_{ij}^{2\omega}$ are defined by (A.9) to (A.11) with ω replaced with 2ω and with $j=s,p$.

References

- [1] J. F. McGilp, *Surf. Rev. Lett.* **6**, 529 (1999).
- [2] T. F. Heinz, in *Nonlinear Surface electromagnetic Phenomena*, ed. H. –E. Ponath and G. I. Stegeman (Elsevier, Amsterdam, 1991) p. 353.
- [3] Y. R. Shen, *The Principles of Nonlinear Optics* (Wiley Interscience, New York, 1984) Chap. 25.
- [4] Y. R. Shen, *J. Vac. Sci. Technol.* **B3**, 1464 (1985).
- [5] C. Yamada and T. Kimura, *Phys. Rev. Lett.* **70**, 2344 (1993).
- [6] C. Yamada and T. Kimura, *Phys. Rev.* **B49**, 14372 (1994).
- [7] D. J. Bottomley, G. Lüpke, J. G. Mihaychuk, and H. M. van Driel, *J. Appl. Phys.* **74**, 6072 (1993).
- [8] V. N. Gridnev, V. V. Pavlov, R. V. Pisarev, A. Kirilyuk, and Th. Rasing, *Phys. Rev.* **B63**, 184407 (2001).
- [9] T. Stehlin, M. Feller, P. Guyot-Sionnest, and Y. R. Shen, *Opt. Lett.* **13**, 389 (1988).
- [10] J. E. Sipe, D. J. Moss, and H. M. van Driel, *Phys. Rev.* **B35**, 1129 (1987).
- [11] S. V. Govorkov, N. I. Koroteev, I. L. Shumay, and V. V. Yakovlev, *J. Opt. Soc. Am.* **B8**, 1023 (1991).
- [12] N. Bloembergen, *Nonlinear Optics* (Addison-Wesley Publishing, Redwood City, 1992) Chap. 1.
- [13] K. Kumagai, G. Mizutani, H. Tsukioka, T. Yamauchi, and S. Ushioda, *Phys. Rev.* **B48**, 14488

(1993).

[14] E. Kobayashi, G. Mizutani, and S. Ushioda, Jpn. J. Appl. Phys. **36**, 7250 (1997);

[15] S. Nakamura, K. Matsuda, T. Wakasugi, E. Kobayashi, G. Mizutani, S. Ushioda, T. Sekiya, and S. Kurita, J. Lumin. **87-89**, 862 (2000).

[16] G. Mizutani, N. Ishibashi, S. Nakamura, T. Sekiya, and S. Kurita, Int. J. Mod. Phys. B15, 3873 (2001).

[17] E. Kobayashi, K. Matsuda, G. Mizutani, and S. Ushioda, Surf. Sci. **427-428**, 294 (1999).

[18] G. Vrillet, S. K. Lee, D. McStay, P. K. J. Robertson, Appl. Surf. Sci. 222, 33 (2004).

[19] E. Kobayashi, T. Wakasugi, G. Mizutani, and S. Ushioda, Surf. Sci. **402-404**, 537 (1998);

Later we found that there was a small amount of Si contamination on on the sample surfaces used in papers 14 and 14a, so that some of the SH intensity patterns in Fig. 4 in the present paper should replace the corresponding patterns in these papers.

[20] H. Sano, G. Mizutani, W. Wolf, and R. Podloucky, to be published.

[21] E. Asari, W. Hayami, and R. Souda, Appl. Surf. Sci. **167**, 169 (2000).

[22] H. Onishi and Y. Iwasawa, Surf. Sci. **313**, L783 (1994).

[23] Y. W. Chung, W. J. Lo and G. A. Somorjai, Surf. Sci. **64**, 588 (1977).

[24] M. A. Henderson, Surf. Sci. **355**, 151 (1996).

[25] U. Diebold, Surf. Sci. Reports **48**, 53 (2003).

[26] P. Guyot-Sionnest, W. Chen, and Y. R. Shen, Phys. Rev. **B33**, 8254 (1986).

- [27] H. Sano and G. Mizutani, e-J. Surf. Sci. Nanotech. **1**, 57 (2003).
- [28] K. M. Glassford and J. R. Chelikowsky, Phys. Rev. **B46**, 1284 (1992).
- [29] Shang-Di Mo and W. Y. Ching, Phys. Rev. **B51**, 13023 (1995).
- [30] D. Vogtenhuber, R. Podloucky, A. Neckel, S. G. Steinemann, and A. J. Freeman, Phys. Rev. **B49**, 2099 (1994).
- [31] M. Ramamoorthy, D. Vanderbilt, and R. D. King-Smith, Phys. Rev. **B49**, 16721 (1994).
- [32] P. Reinhardt and B. A. Hess, Phys. Rev. **B50**, 12015 (1994).
- [33] S. P. Bates, G. Kresse, and M. J. Gillan, Surf. Sci. **385**, 386 (1997).
- [34] P. K. Schelling, N. Yu, and J. W. Halley, Phys. Rev. **B58**, 1279 (1998).
- [35] N. M. Harrison, X. -G. Wang, J. Muscat, and M. Scheffler, Faraday Discuss. **114**, 305 (1999).
- [36] H. Sano, G. Mizutani, W. Wolf, and R. Podloucky, Phys. Rev. **B66**, 195338 (2002).
- [37] L. Hedin and B. I. Lundqvist, J. Phys. **C4**, 2064 (1971).
- [38] L. Reining, R. Del Sole, M. Cini, and J. G. Ping, Phys. Rev. **B50**, 8411 (1994).
- [39] B. S. Mendoza, A. Gaggiotti, and R. Del Sole, Phys. Rev. Lett. **81**, 3781 (1998).
- [40] M. Murao, E. Kobayashi, and G. Mizutani, Technical Digest of CLEO/Pacific Rim 2001, pp. II146-147 (2001)
- [41] F. A. Grant, Rev. Mod. Phys. **31**, 646 (1959).
- [42] M. W. Ribarsky: in *Handbook of Optical Constants of Solids*, ed. E. D. Palik (Academic Press, San Diego, 1985) p. 795.

- [43] H. W. K. Tom, T. F. Heinz, and Y. R. Shen, Phys. Rev. Lett. **51**, 1983 (1983).
- [44] J. Goniakowski and M. J. Gillan, Surf. Sci. **350**, 145 (1996).
- [45] J. Gopalakrishnan, K. Ramesha, K. K. Rangan, and S. Pandey, J. Solid State Chem. **148**, 75 (1999).
- [46] R. Heise, R. Courths, and S. Witzel, Solid State Commun. **84**, 599 (1992).
- [47] P. J. Hardman, G. N. Raikar, C. A. Muryn, G. van der Laan, P. L. Wincott, G. Thornton, D. W. Bullett, and P. A. D. M. A. Dale, Phys. Rev. **B49**, 7170 (1994).
- [48] A. K. See, M. Thayer, and R. A. Bartynski, Phys. Rev. **B47**, 13722 (1993).

Figure Captions

Fig. 1 Model of the atomic arrangement of a clean $\text{TiO}_2(110)$ surface. Bridging oxygen atoms α -O's and the nearest neighbor titanium atoms γ -Ti's form Ti-O-Ti-O- zigzag chains.

Fig. 2 Block diagram of the experimental set-up for SHG measurements. OPO, BS, PMT, Amp, and A/D represent the optical parametric oscillator, beam splitter, photomultiplier tube, amplifier, and analog-to-digital converter, respectively.

Fig. 3 Dielectric model of a three-layer system used in the phenomenological analysis. The dielectric constants for the electric fields in the directions indicated by arrows are shown for the two models. Models 1 and 2 are for the $\text{TiO}_2(110)$ and (001) faces, respectively. The c-axis or [001] direction of bulk TiO_2 crystal lies in directions 1 and 3 in Models 1 and 2, respectively. In the Appendix of this paper the coordinate (1,2,3) is rewritten as (x,y,z) in order to avoid confusion.

Fig. 4 Measured SH intensity patterns from a $\text{TiO}_2(110)$ face as a function of the sample rotation angle ϕ around its surface normal. The incident angle is 45° . The input and the output polarizations are shown in the figure, such as P_{in}/S_{out} for p-polarized input and s-polarized output. The SH photon energies are shown in the left. The SH intensity is plotted in the radial direction.

The scale maximum of the intensity is shown in an arbitrary unit to the right of each pattern, and the patterns for the same SH photon energy are drawn in a common unit. The zero degree corresponds to the configuration when the plane of incidence includes the [001] direction on the sample. Small alphabet from *a* to *e* in circles indicate the configurations for the spectroscopic measurements in Fig. 7.

Fig. 5 Measured SH intensity patterns from the TiO₂(001) face as a function of the sample rotation angle ϕ around its surface normal. The incidence angle is 45°. The input and the output polarizations are shown in the figure, such as Pin/Sout for p-polarized input and s-polarized output. The SH photon energies are shown in the left. The SH intensity is plotted in the radial direction. The scale maximum of the intensity is shown in an arbitrary unit to the right of each pattern, and the patterns for the same SH photon energy are drawn in a common unit. The zero degree corresponds to the configuration when the plane of incidence includes the [100] direction on the sample.

Fig. 6 The SH intensity from the TiO₂(001) face as a function of the incident angle at the SH photon energy of $2\eta\omega = 4.66\text{eV}$. The dots with error bars represent SH intensity from the TiO₂(001) face divided by the SH intensity from the GaAs(001) as a function of the incident angle. The solid curves are calculated SH intensity for three important nonlinear susceptibility elements.

Fig. 7 The reflected SH intensity from the rutile $\text{TiO}_2(110)$ face as a function of the SH photon energy $2\eta\omega$ in air. The polarization combination and the sample rotation angle adopted for each panel are indicated in the figure and were also indicated in Fig. 4 using the alphabet from a to e in circles. The solid curves are guide to the eye. The arrow indicates the band gap of the bulk rutile TiO_2 .

Fig. 8 The reflected SH intensity from the rutile $\text{TiO}_2(001)$ face as a function of the SH photon energy $2\eta\omega$ in air. The polarization combination is Pin/Pout and the plane of incidence is parallel to the $[100]$ direction. The solid curve is a guide to the eye. The arrow indicates the band gap of the bulk rutile TiO_2 .

Fig. 9 SH intensity patterns obtained by theoretical calculation when one of the surface nonlinear susceptibility elements $\chi_{Sijk}^{(2)(110)}$ is set equal to a certain common value and all the other elements are set equal to zero. The SH intensity is normalized by the maximum intensity in each pattern and the maximum intensity is shown below the pattern. The intensities are in arbitrary, but common units. The suffices i, j , and k of the surface nonlinear susceptibility $\chi_{Sijk}^{(2)(110)}$ refer to the axis frame defined in Fig. 1.

Fig. 10 SH intensity patterns obtained by theoretical calculation when one of the surface nonlinear

susceptibility elements $\chi_{sijk}^{(2)(001)}$ is set equal to a certain common value and all the other elements are set equal to zero. The SH intensity is normalized by the maximum intensity in each pattern and the maximum intensity is shown below the pattern. The intensities are in arbitrary, but common units. As the suffices of the surface nonlinear susceptibility elements $\chi_{sijk}^{(2)(001)}$, 1 indicates the direction [100] and 3 indicates the direction [001].

Fig. 11 SH intensity patterns obtained by theoretical calculation when one of the surface nonlinear susceptibility elements Γ_{ijkl} is set equal to a certain common value and all the other elements are set equal to zero. The SH intensity is normalized by the maximum intensity in each pattern and the maximum intensity is shown below the pattern. The intensities are in arbitrary, but common units. The suffices of the bulk nonlinear susceptibility Γ_{ijkl} refer to the crystallographic axis of bulk TiO₂.

Fig. 12 SH intensity patterns obtained by theoretical calculation fitted to the experimental data of Fig. 4a to d (a to d) and to those of Fig. 5a to d (e to h).

Fig. 13 Calculated surface (a-d) and bulk (e-h) contributions in the SH intensity separated from the patterns in Fig. 12 a to d.

Fig. 14 Calculated SH intensity as a function of the SH photon energy for Pin/Pout (solid line) and Sin/Pout (dashed line) polarization combinations for the relaxed TiO₂(110) surface. The plane of incidence is parallel to the [001] direction. Empty and gray circles are the measured SH intensity and are the same data as those shown in Fig. 7a and e. The scale of the measured data is adjusted to match the calculated data.

Fig. 15 SH intensity as a function of the sample rotation angle ϕ around the surface normal at the SH photon energy $2\eta\omega=4.0\text{eV}$ obtained by the *ab initio* calculation. The scales in the radial direction are in an arbitrary but common unit.

Table I The ratios of SH intensities of the $\text{H}_2\text{O}/\text{TiO}_2(110)$ face to the $\text{H}_2\text{O}/\text{TiO}_2(001)$ face

SH Photon energy $2\eta\omega$	(110) : (001)
3.34eV	1.77 : 1
3.65eV	0.83 : 1
4.00eV	1.98 : 1
4.66eV	1.41 : 1

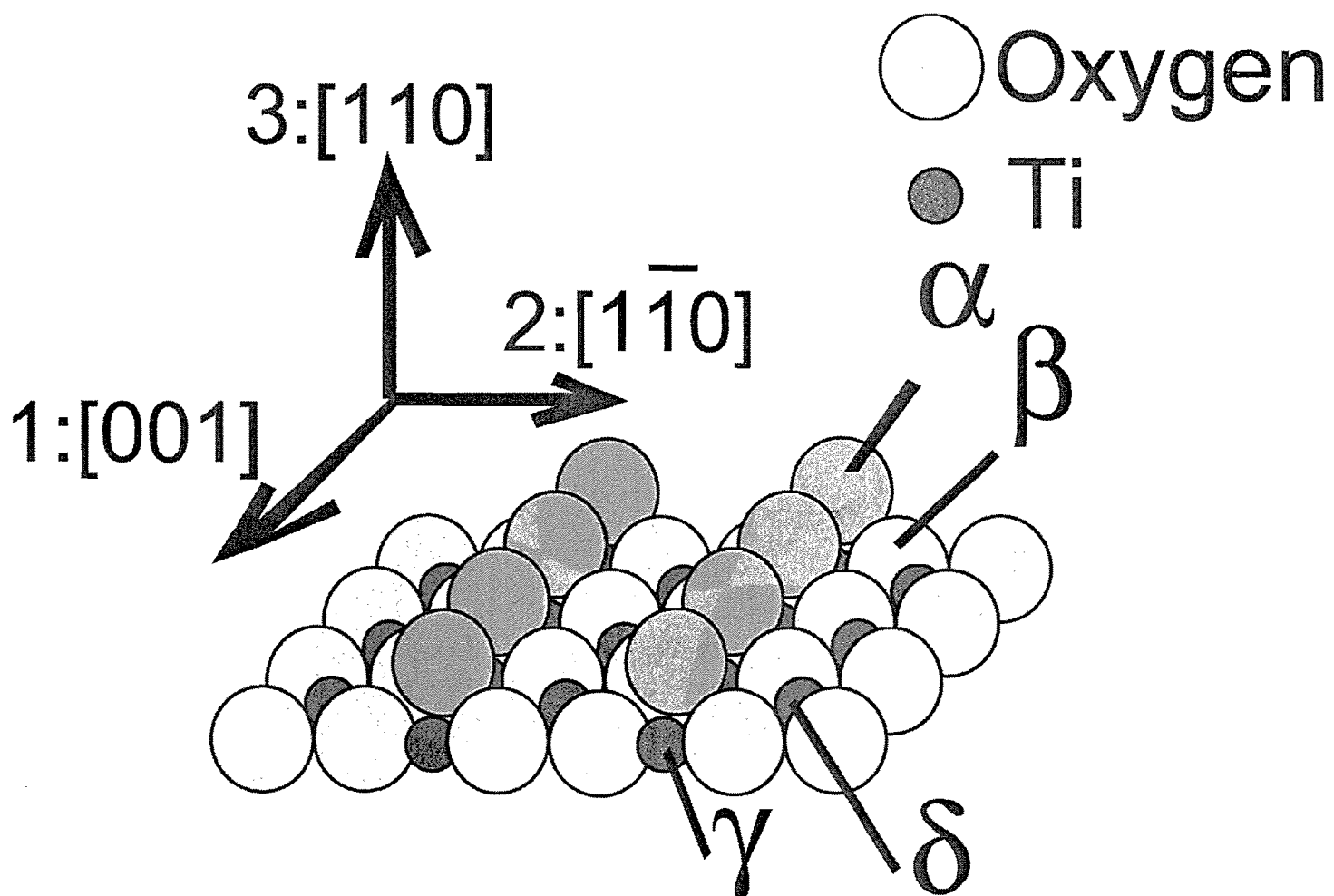


Figure 1 Omote et al.

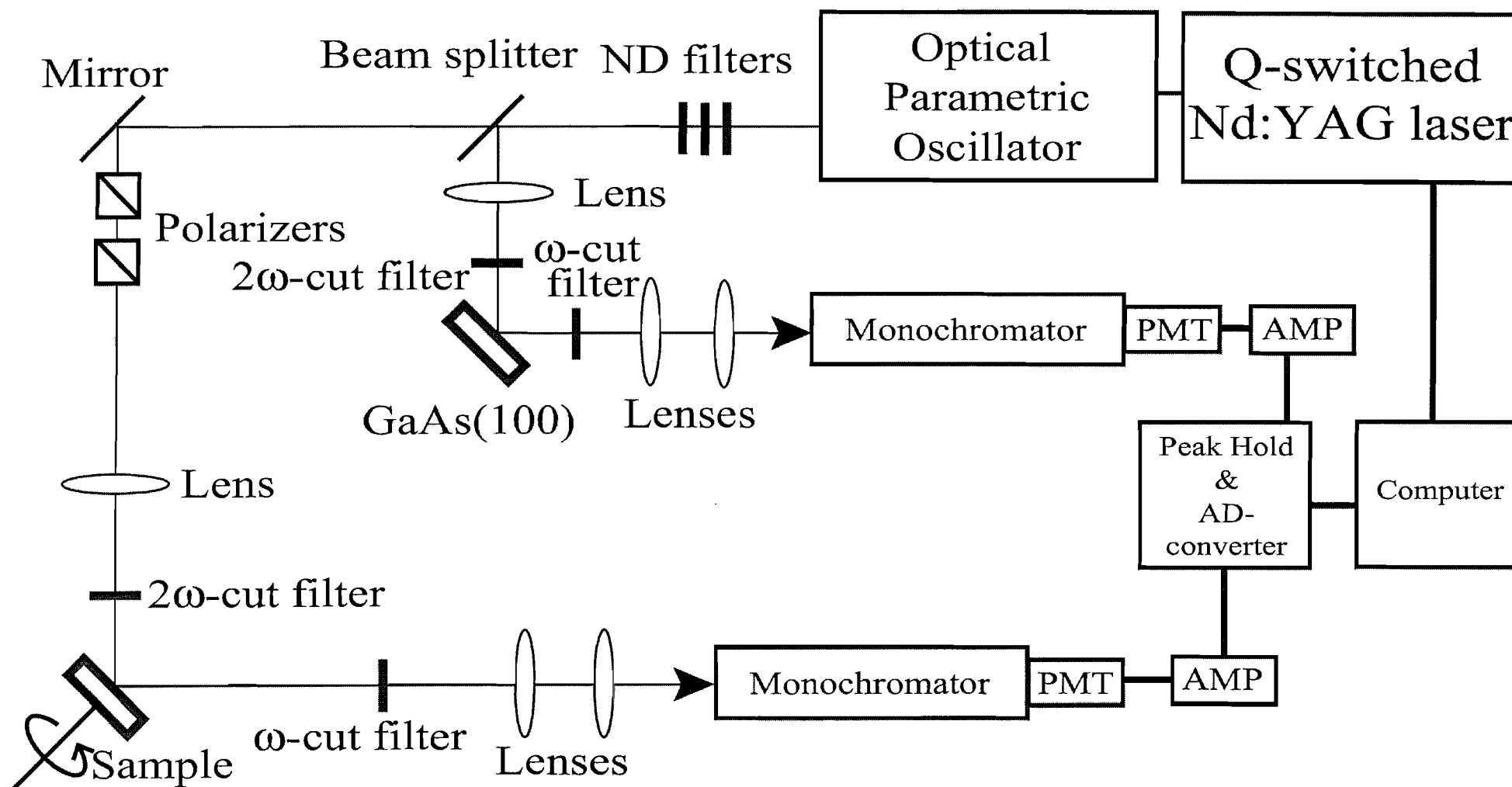


Figure 2 Omote et al

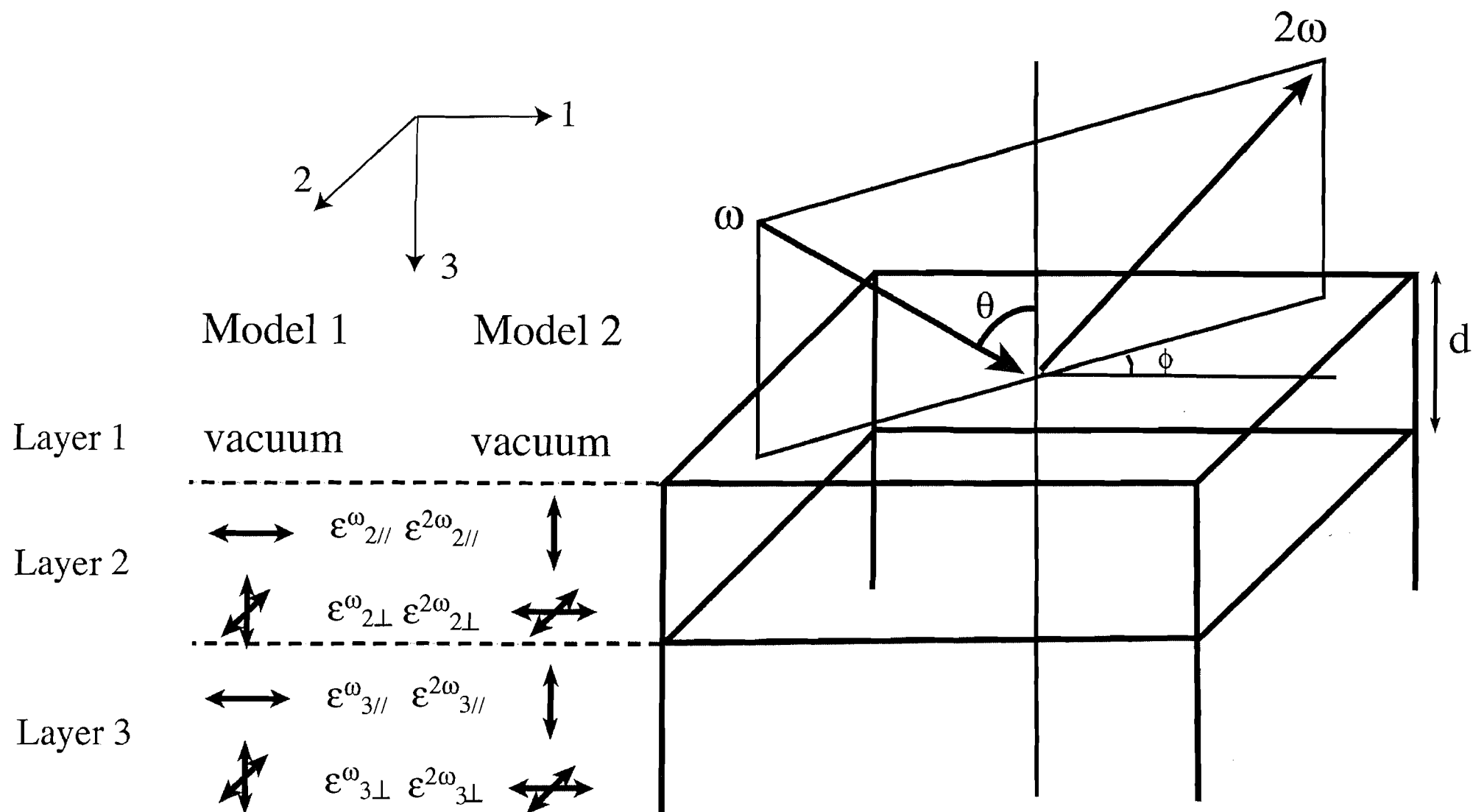


Figure 3 Omote et al

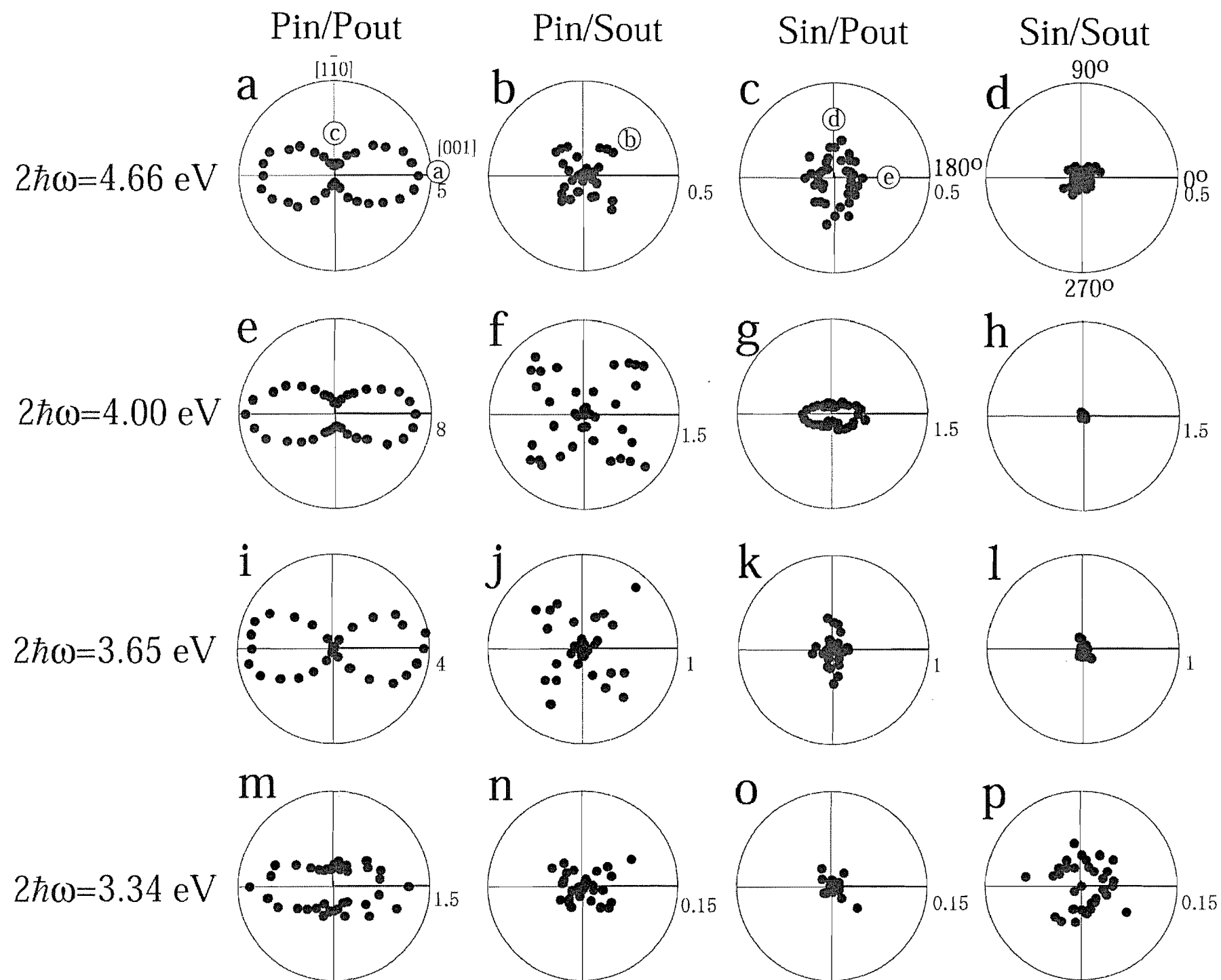


Figure 4 Omote et al.

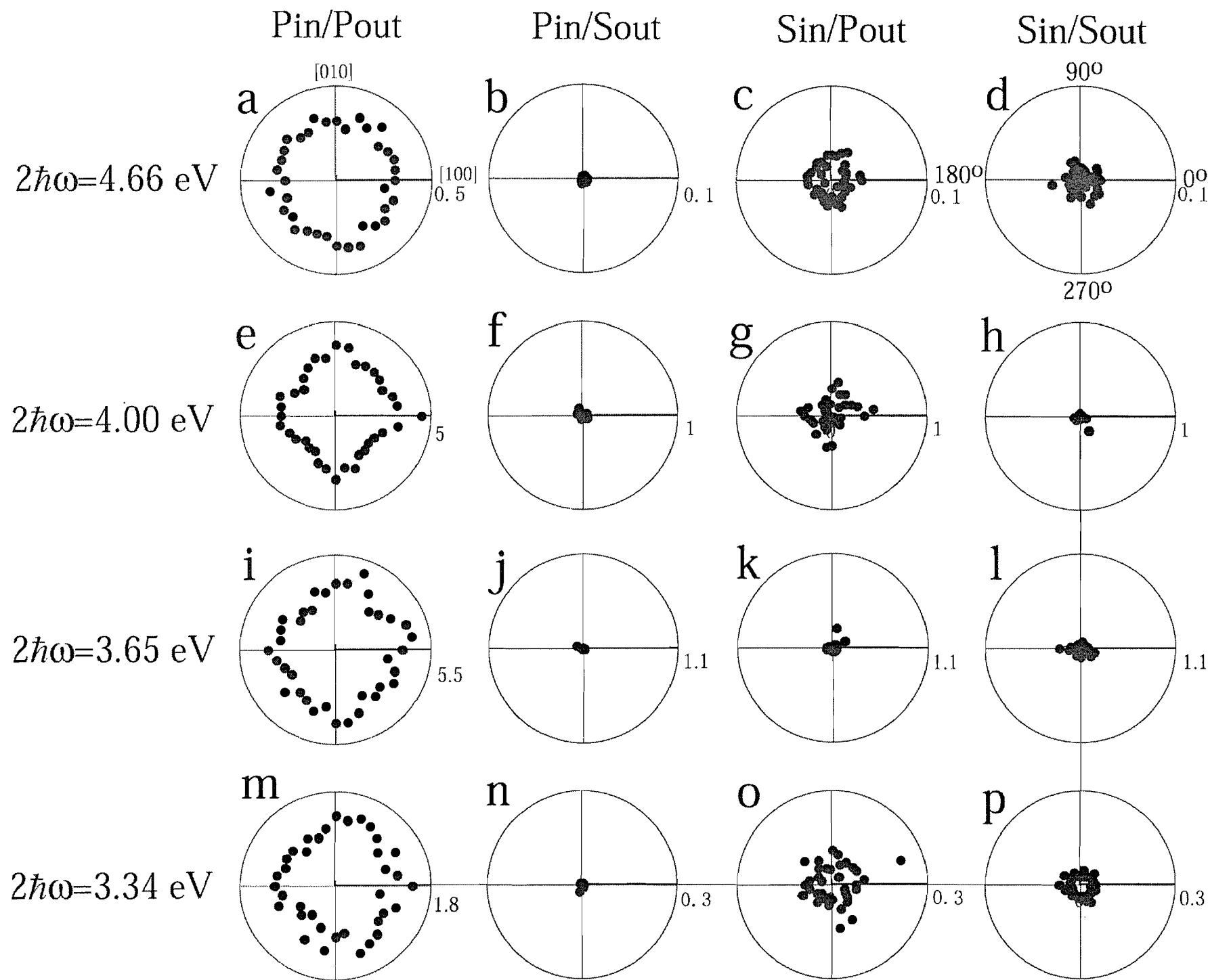


Figure 5 Omote et al.

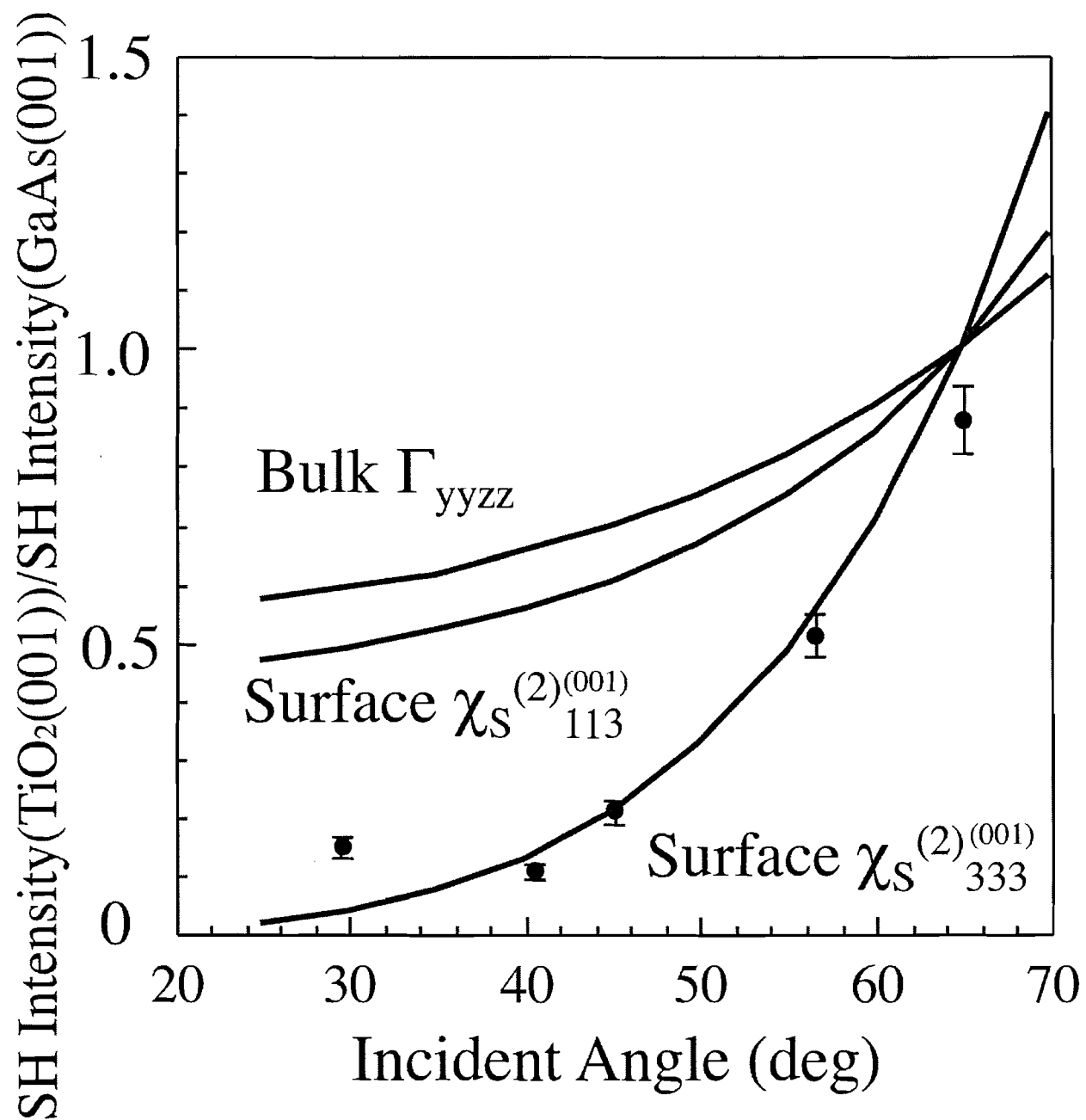


Figure 6 Omote et al

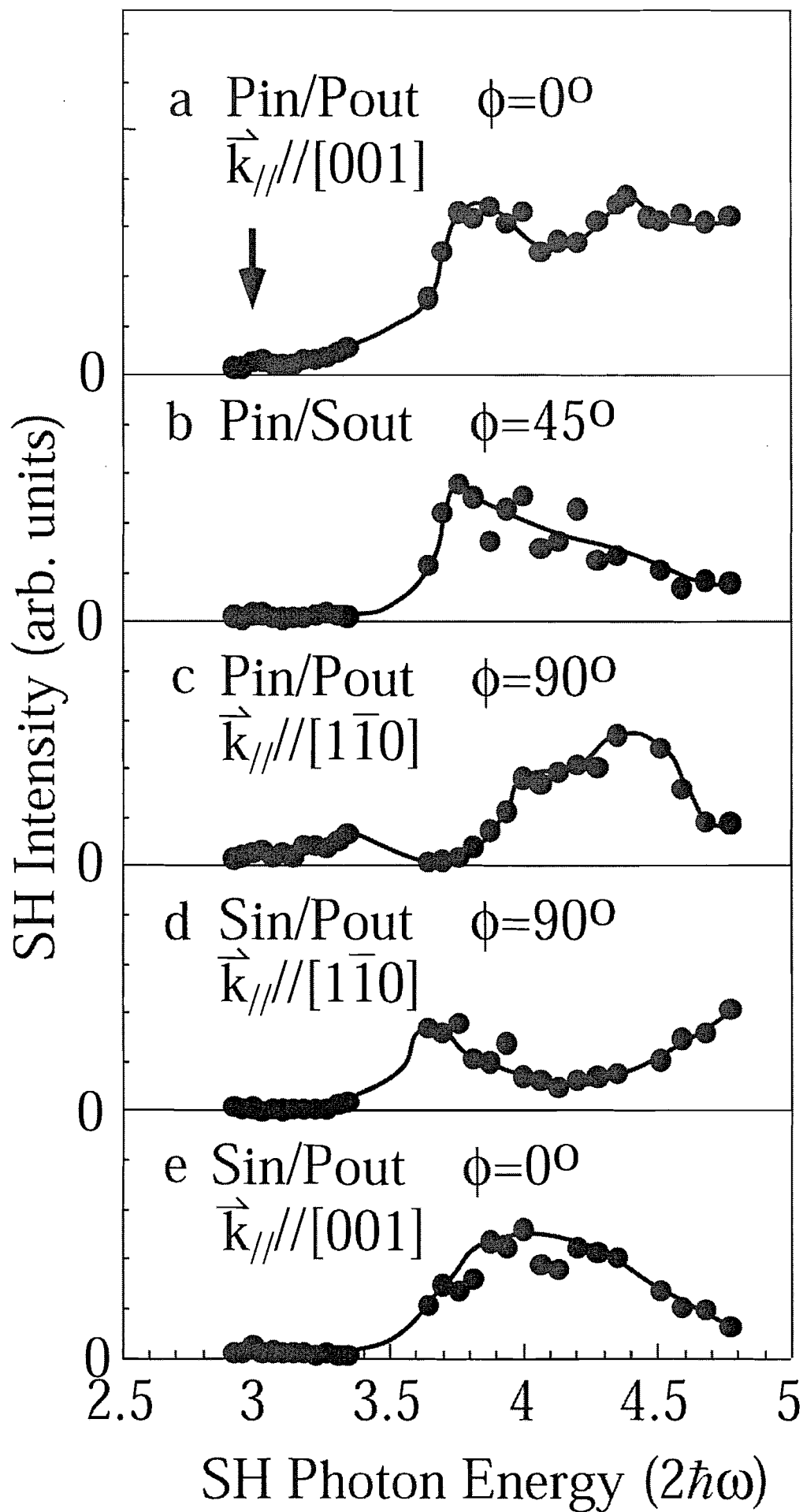


Figure 7 Omote et al.

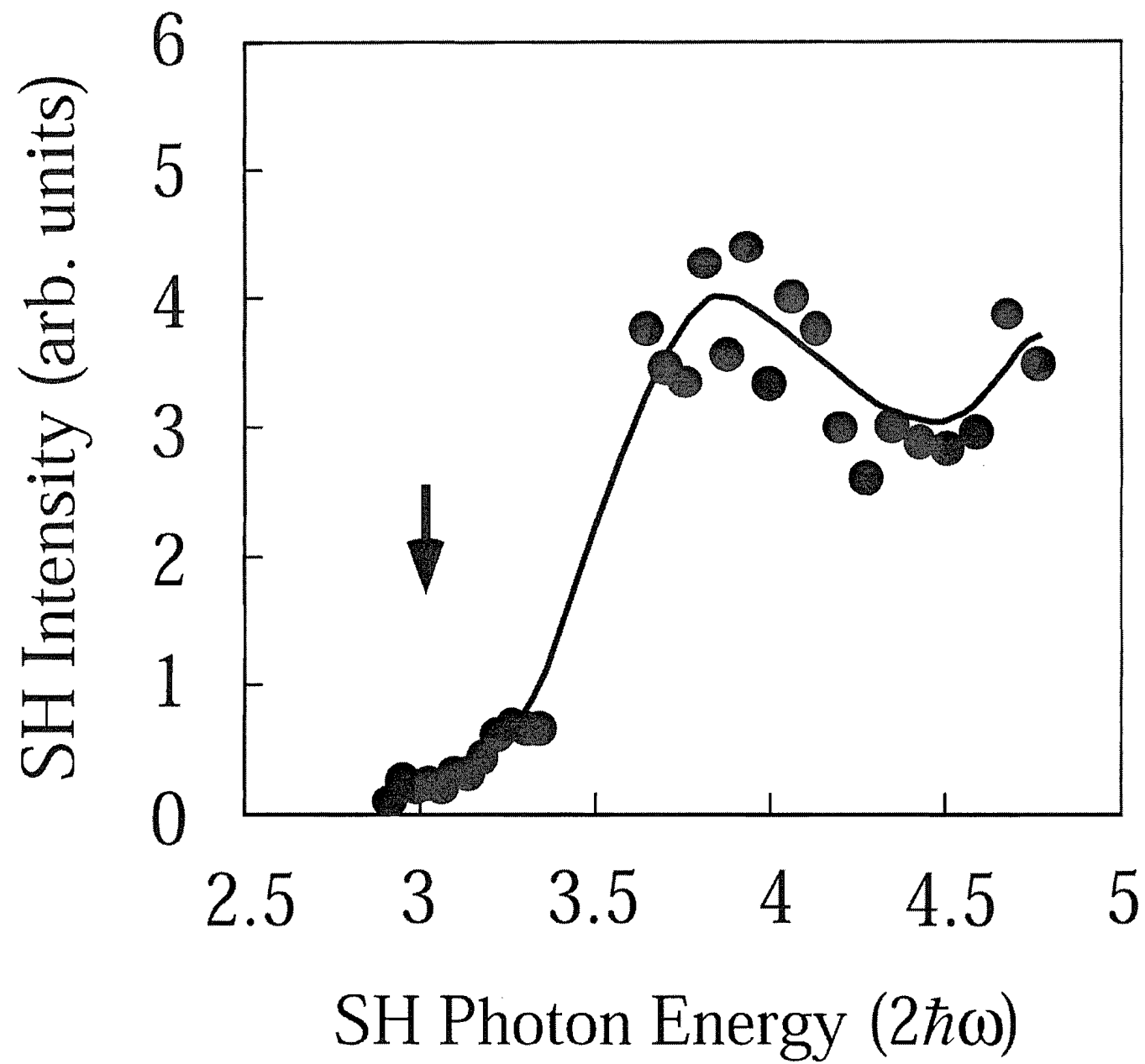


Figure 8 Omote et al.














ijk of $\chi^{(2)(110)}_{Sijk}$	Pin/Pout	Pin/Sout	Sin/Pout	Sin/Sout
113	 1.392	 0.221	0	0
223	 1.953	 0.345	0	0
311	 2.269	 0.004	 1.043	 0.002
322	 2.277	 0.004	 2.002	 0.003
333	 51.165	0	0	0

Figure 9 Omote et al





ijk of $\chi^{(2)(001)}_{Sijk}$	Pin/Pout	Pin/Sout	Sin/Pout	Sin/Sout
113	 2.016	0	0	0
311	 2.295	0	 1.486	0
333	 32.773	0	0	0

Figure 10 Omote et al





































































	(110) $\begin{array}{c} [1\bar{1}0] \\ \uparrow \\ [001] \end{array}$				(001) $\begin{array}{c} [100] \\ \uparrow \\ [010] \end{array}$			
ijkl of Γ_{ijkl}	Pin Pout	Pin Sout	Sin Pout	Sin Sout	Pin Pout	Pin Sout	Sin Pout	Sin Sout
xxxx	 0.210	 0.243	 0.350	 0.043	 2.378	 0.103	 0.386	 0.068
zzzz	 1.092	 0.078	 0.040	 0.045	 0.001	0	0	0
yyzz	 0.107	 0.141	 0.083	 0.090	 1.554	0	0	0
zzyy	 1.685	 0.121	 0.061	 0.069	 0.002	0	0	0
zyyz	 1.685	 0.130	 0.049	 0.057	 0.002	0	0	0
yzzy	 0.108	 0.141	 0.083	 0.090	 1.553	0	0	0
yzyz	 1.821	 0.141	 3.416	 0.082	 0.006	0	0	0
zyzy	 0.125	 0.131	 1.045	 0.075	 0.596	0	 0.383	0
xxyy	 0.174	 0.024	 0.350	 0.030	 0.593	 0.103	 0.386	 0.068
xyxy	 9.340	 0.733	 0.350	 0.027	 0.593	 0.103	 1.544	 0.068
xyyx	 0.174	 0.030	 0.350	 0.018	 0.593	 0.103	 0.386	 0.068

Figure 11 Omote et al

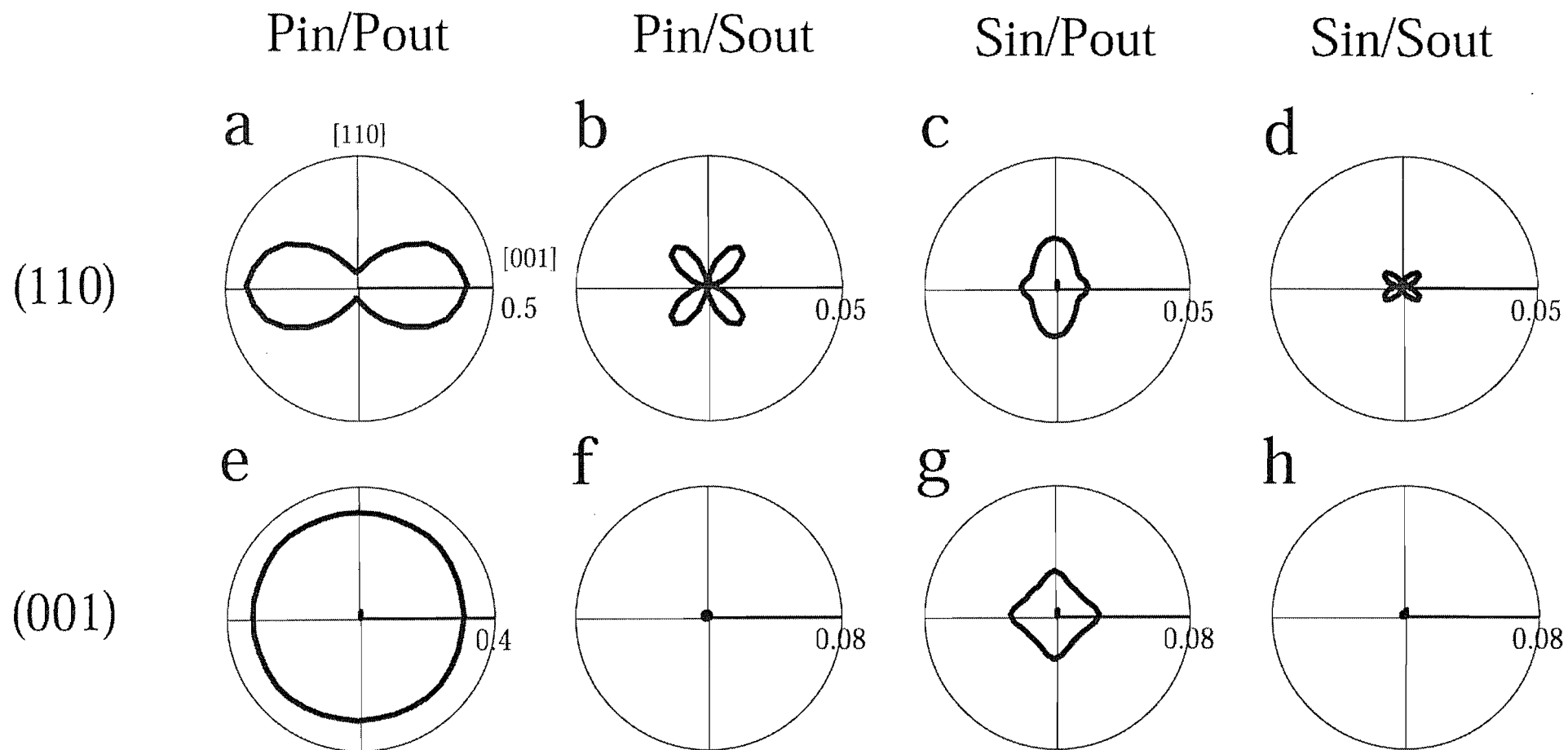


Figure 12 Omote et al.

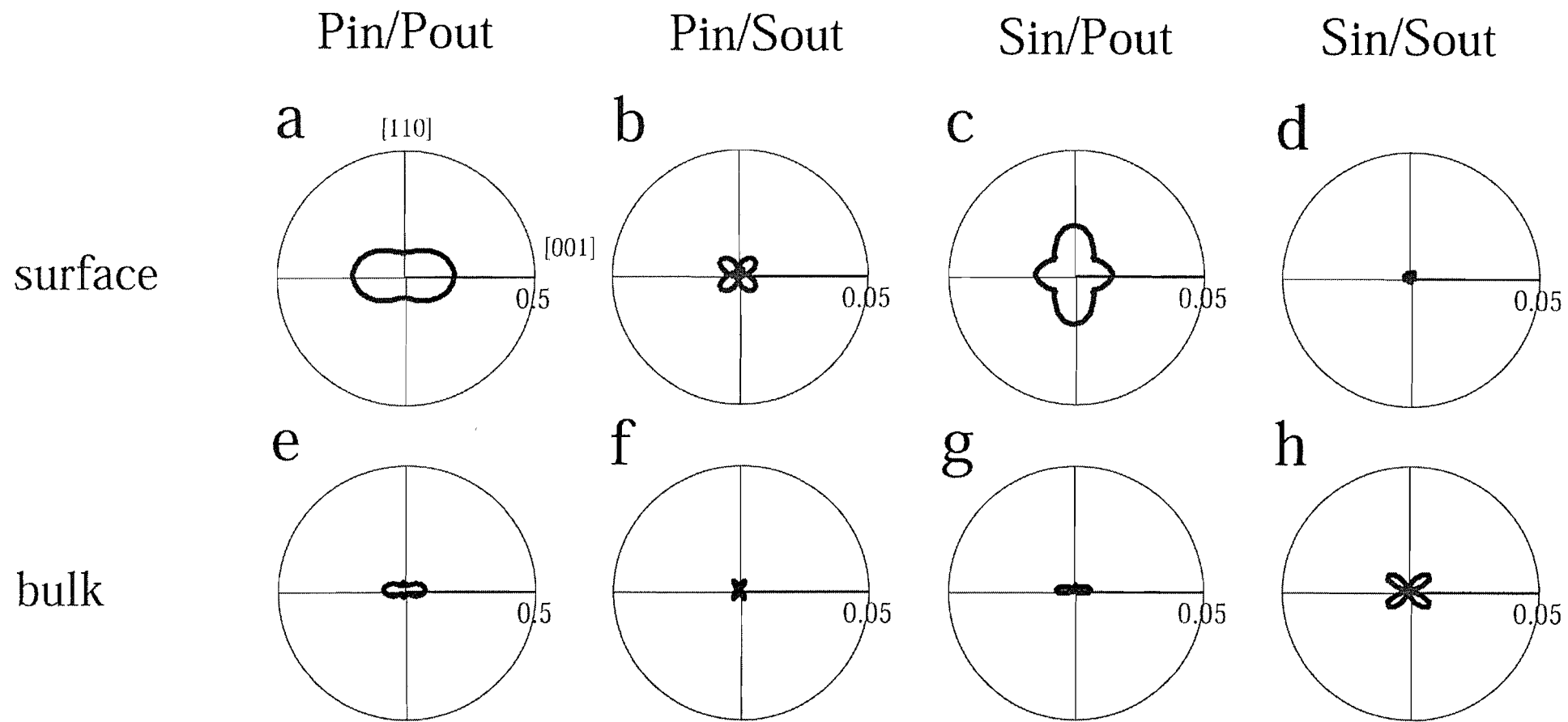


Figure 13 Omote et al.

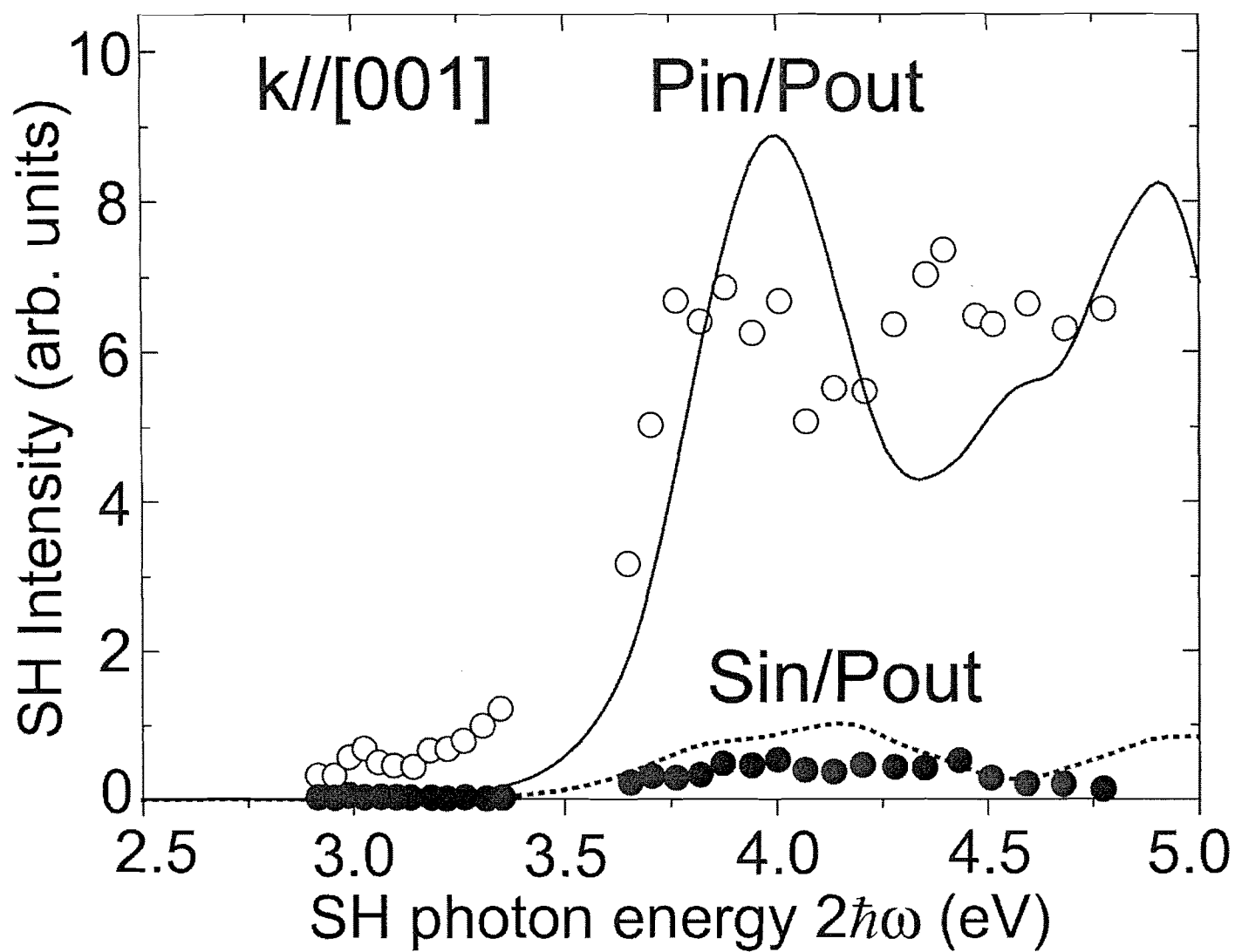


Figure 14 Omote et al

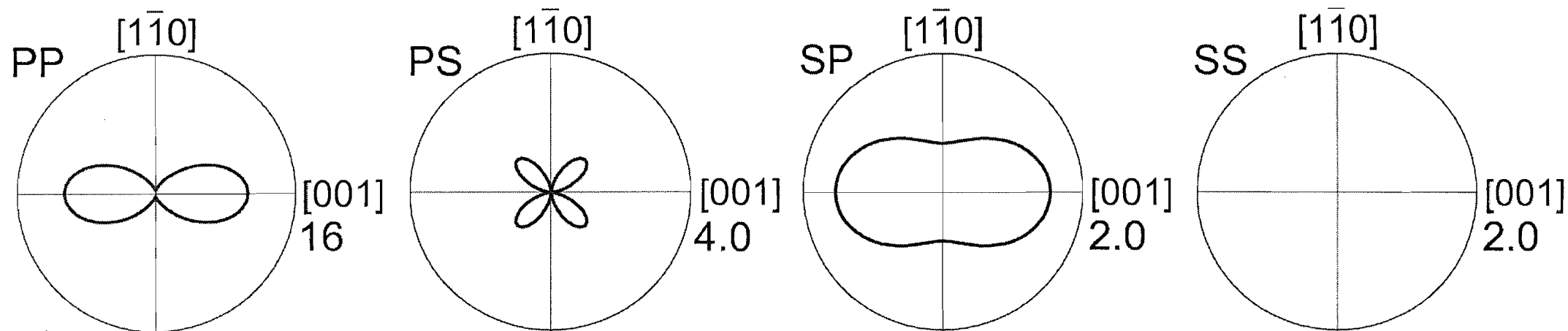


Figure 15 Omote et al